AN ABSTRACT OF THE THESIS OF

Rigel Woodside for the degree of
Master of Science in
Mechanical Engineering presented
On January 22, 2008
Title: Investigating Arc Behavior in a DC Vacuum Arc Remelting Furnace Using Magnetic Flux Density Measurements

Abstract approved:

Paul E. King

The behavior of a metal vapor plasma arc in a vacuum arc remelting (VAR) furnace is believed to contribute to the formation of defects in reactive metal and super-alloy ingots. Industry standard instrumentation, which includes electric current and voltage measurements, can asses the stability of an arc but cannot predict the location of an arc. It is known that Maxwell's equations predict a magnetic flux density at a distance from an arc. It is shown that a single arc's location can be uniquely determined in a cross section by using an externally mounted 2-axis Hall Effect magnetic flux density sensor provided that the system's electric current is also measured and the geometry of the VAR furnace is known. The solution is based on the Biot-Savart Law with finite element modeling assisting the analysis. The methodology is validated using controlled, static experiments. The measurement system is deployed on a small scale, experimental VAR furnace to investigate arc behavior. Results from VAR operation show a time averaged arc distribution that does not significantly change over the course of a melt. By comparing the results from multiple sensors, observed arc motions are categorized as being either retrograde or sympathetic. The former is characterized by large periodic motions, and the latter either small random motions or motions associated with an event such as a liquid metal drip short. Significant alternating currents are found to exist in the DC VAR furnace. A magnetostatic single arc model is not sufficient to describe the current distribution in the VAR furnace at an instant but it may be an effective means to detect quasi static non-axisymmetry or slow time varying current profile changes during VAR operation.

Investigating Arc Behavior in a DC Vacuum Arc Remelting Furnace Using Magnetic Flux Density Measurements

by

Rigel Woodside

A THESIS

submitted to

Oregon State University

in partial fulfillment of

the requirements for the

degree of

Master of Science

Presented January 22, 2008

Commencement June 2008

Master of Science thesis of Rigel Woodside

Presented on January 22, 2008

APPROVED:

Major Professor, representing Mechanical Engineering

Head of the School of Mechanical, Industrial, & Manufacturing Engineering

---

Dean of the Graduate School

I understand that my thesis will become part of the permanent collection at Oregon State University libraries. My signature below authorizes release of my thesis to any reader upon request.

Rigel Woodside, Author

ACKNOWLEDGEMENTS

I would like to thank several people that helped made this work possible. Thanks to Dr. Paul King who is the Research Program Leader for the Process Development Division at the United States DOE, National Energy Technology Laboratory (NETL) in Albany, Oregon. He introduced me to the topic and gave me guidance and support throughout the process. Dr. Paul Jablonski, NETL Metallurgist, for his VAR furnace operation knowledge, and the excellent supporting photography contained in this document. Ed Argetsinger, NETL Engineering Technician, for preparing and operating all of the VAR experiments. Thanks to the folks at Precision Measurements and Instrumentals Corporation whom I worked with for 5 years, learning the science of applying measurement systems. Also, my instructors at Oregon State University whom helped me expand my horizons into other fields. I'd like to thank my wife, Jasmin Woodside, for her support and understanding especially over the last few months during the preparation of this manuscript.

This work was supported by a cooperative research and development agreement (CRADA) between the United States Department of Energy and the Specialty Metals Processing Consortium (SMPC).

TABLE OF CONTENTS

LIST OF FIGURES

LIST OF FIGURES (continued)

Figure Page

LIST OF FIGURES (continued)

Figure Page

LIST OF TABLES

Investigating Arc Behavior in a DC Vacuum Arc Remelting Furnace Using Magnetic Flux Density Measurements

Rigel Woodside

Introduction

Vacuum arc remelting (VAR) is a metallurgical casting process used to improve a material's chemical and physical homogeneity. The input material is referred to as a consumable electrode. Electrical power heats the consumable electrode by means of an electric arc, and gravity works to transport the melting material into the water cooled copper crucible. The output product is a uniform, cylindrical ingot that has a larger diameter than the input. A VAR furnace is especially desirable if the material is reactive to atmospheric gases at elevated temperatures, sensitive to alloy segregation during cooling, and conducts electrical current. So the key characteristics of VAR are vacuum pressures, fast cooling times, and an electric arc as the heating source.

The benchmark condition for producing a quality ingot has been shown to be a diffuse arc.[1] This means arc current is uniformly spatially distributed as a function of time, which results in a quasi steady heat input to the ingot melt pool. Currently, commercial VAR furnaces monitor a variety of parameters but there is no capability available to monitor and track arcs on these furnaces. During VAR operation non-diffuse arcs are more likely to result in material defects in the ingot. These defects in turn are sites that tend to result in fatigue related failures in materials. This is especially of concern in the aviation industry which relies on high performance, high temperature metals for turbine engines where the VAR is the primary melting process for rotating parts.

The principle goal of this research was to develop a measurement system capable of monitoring VAR arc behavior. A constraint of the system was the desire to be able to use it on existing furnaces. So the developed system needed to be non-invasive, versatile and capable of real time functionality.

To this end, monitoring arc behavior is achieved by measuring the system's electric current in the usual manner coupled with externally mounted 2-axis hall effect sensors which measure the magnetic flux density. This takes advantage of the well known Maxwell-Ampere equation which relates an electric current density to a

diverging magnetic flux density. Thus, a moving current causes a change in magnetic flux at a distance. Unique to this study is the developed analysis which provides a foundation for future study of furnace arcs at the National Energy Technology Laboratory (NETL) in Albany, Oregon.

VAR Operation

The VAR furnace was first utilized to melt metals in the 19th century, primarily in small laboratory scale furnaces. In the 1940's the VAR furnace became widespread because of the need to produce aircraft engines. Today, it remains one of the most utilized processes for the production of Titanium, Super Alloys, Stainless Steel and high strength steel forging stock.

A VAR furnace comes in a variety of sizes, capable of producing ingots a fraction of a meter in diameter to ingots in excess of 1 meter in diameter.

Figure 1, on the following page, shows a schematic of a typical VAR furnace.

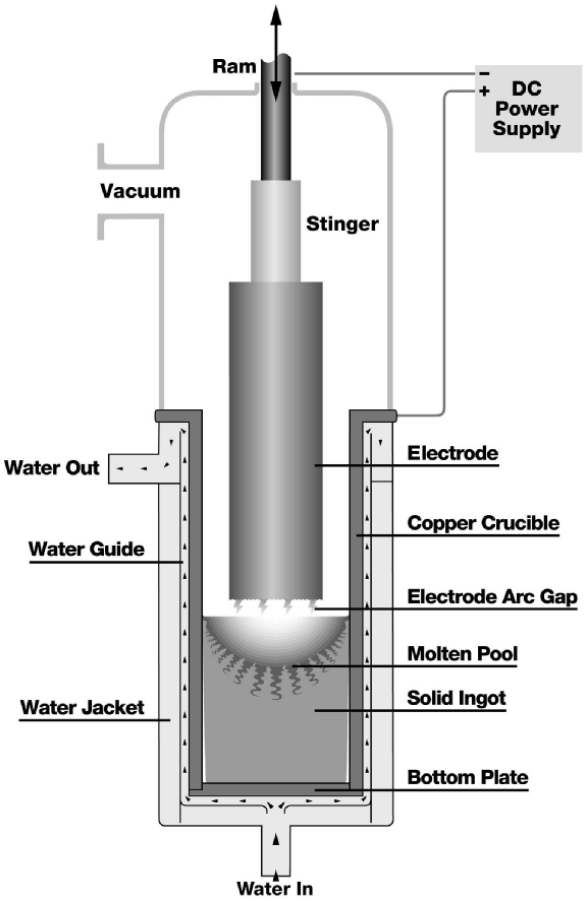

Figure 1 : Typical VAR schematic (courtesy ATI Allvac)

From top to bottom the components of a typical VAR furnace are as follows. A manually or computer controlled servo motor and gears are used to control the up and down motion of the ram. The ram is water cooled and enters the vacuum chamber by a mechanical feed through. A Stinger is an expendable connection that bridges the ram to a machined thread on the electrode. The electrode is referred to as consumable because it is made of the material that is to be melted. The electrode could be continuous bar stock, or it could be multiple pieces welded together. The VAR process is often repeated several times, both to increase the homogeneity of the material, and to increase the diameter of the cylindrical ingot.

An electrical current induces a metal vapor plasma arc which heats the electrode and gravity works to transfer metal drops into the forming ingot. The ingot solidifies in a water cooled copper cylinder having a diameter slightly larger than the electrode. The copper crucible is sometimes made with the top opening slightly larger than the bottom, to ease removal of the ingot after melting is finished. Water cooling of the crucible is required because copper has a lower melting point than the material being melted.

A vacuum pump keeps pressures in the furnace in the millitorr range. Direct current usually supplies the power in VAR operation. The source for this is often a bank of DC supplies hooked up in parallel. In VAR a circuit is created with the electrode and crucible hooked up to opposite sides of the power supply. Thus, the material being melted has to be a good conductor of electricity. In a circuit view of the system the electrode gap (arc region) can be thought of as a variable resistor. A large scale commercial VAR might operate at 40,000 Amps with a 40 Volt drop across the electrode gap region.

Many VAR furnaces are referred to as being coaxial. Figure 1 shows a coaxial set-up as the current flowing in the ingot is in the opposite direction of the current flow in the crucible. The net effect is a cancellation of the magnetic field outside the furnace, as can be visualized using the right hand rule. Also, care is often taken to ensure that the power cables to the furnace also operate in this coaxial manner. The reason for the coaxial power is that it minimizes stray magnetic fields which are known to have an effect on arcs. Still, it should be noted that the coaxial set-up does not eliminate the current generated magnetic fields inside of the crucible.

After set-up, the operation process of VAR begins by applying about 80 Volts to the furnace and striking an arc by briefly touching the electrode to shavings of material placed at the bottom of the crucible. The electrode is raised and the arc spans the gap being conducted by a region of plasma between the electrode and the crucible. The current is then slowly increased until melting is stabilized.

During melting, operational parameters vary depending on the type of melt and the material being melted. In general, there is a bowl shaped pool of molten material in

the middle of the ingot, symmetric about the electrode's axis. A mushy solid/liquid interface exists between the pool and the solidified ingot. As it cools, the ingot pulls away from the crucible wall so that the ingot is suspended in the crucible by a thin section near the top of the ingot.

Figure 2 shows the parameters that are monitored during VAR operation at the National Energy Technology Laboratory (NETL) in Albany, Oregon.

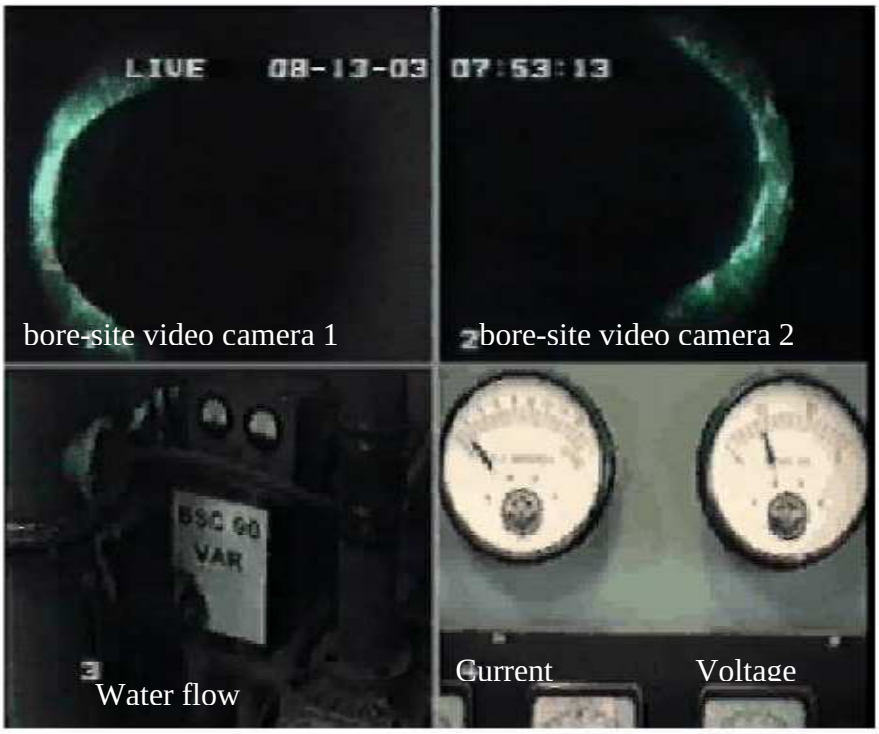

Figure 2 : Parameters monitored during NETL VAR operation

At NETL Albany, two bore site videos, system current, system voltage, and water flow are monitored. The bore site videos are taken from cameras which mount to the top of the furnace and view the melt pool from above and to the sides of the electrode. Control of the VAR process is achieved by varying the applied current and the electrode position.

Operationally, current is the most important parameter. Controlling current has the largest effect on controlling the melting rate for a given material. Voltage measurements are used to decide whether the electrode should be moved up or down. At a given current, a constant voltage is a good indication of a constant gap length. Typically the gap length is held at around 0.5 inches. This operational parameter is about the same regardless of the diameter of the electrode. The video cameras assist the operator by showing part of the top of the melt pool. A uniform melt pool indicates a good melting rate, whereas the presence of slag on the surface could indicate too slow of a melt rate, and the need to increase the applied current. During the process, drip shorts occur which show up as brief spikes in the current. The presence of drip shorts is inevitable as a result of material melting and bridging the gap between the electrode and the ingot surface.

In addition to the already mentioned parameters, large scale commercial VAR furnaces also monitor furnace pressure and electrode weight during operation. Some furnaces also have tilt and side to side control of the position of the electrode. Titanium VAR furnaces also utilize magnetic stirring coils, which will be discussed in more detail later. Most large scale commercial VAR furnaces use automated controllers that try to achieve a constant melt rate. In addition to taking into account the monitoring already described, this also takes into account the thermo physical properties of the melt.

The general goal of Vacuum Arc Remelting operation is to consistently, and efficiently produce quality ingots. The next section discusses why improving the VAR furnace remains relevant, and why behavior and distribution of the arc is important.

Motivations for Arc Characterization

The VAR process is usually repeated several times for a material. The process conditions during the final melt are the most important, and a desire to increase the quality of this melt is what drives research to improve the process.

Applications that particularly need high quality ingots are ones that require performance in extreme and high temperature environments such as jet turbine engines. In this area there remains an increasing demand for even larger single crystal ingots, and alloy systems capable of performing at higher temperatures. Currently, extreme operation temperatures are pushing metal alloy systems to near their mechanical and thermodynamic limits. High quality means low occurrences of defects. Defects are generally areas of the material that differ either in the density or composition from the surrounding material. For example, a defect site may be low in the strength adding alloying element, which results in an area that tends to initiate cracks due to fatigue. The cracks can then propagate, resulting in failure of the part. A failure due to a material defect in a rotating part of a jet turbine engine occurred on United Flight 232 in 1989, in which 110 passengers died.[2]

To avoid operating jet turbine engines containing defective material, a number of non-destructive evaluation techniques are employed. [3] The types of inspection used are categorized as surface, near surface, and subsurface evaluation. Surface evaluation looks for surface-connected heterogeneities using visual inspection, surface roughness measurement, and dye penetrate inspection. Near surface looks for close to surface heterogeneities, using eddy current or magnetic particle inspection. For sub surface, radiography is nearly always utilized. This can successfully locate porosity, density perturbations, and even the condition of internal parts in an assembled turbine. Finally, ultrasonic subsurface inspection has emerged, which is especially attractive for on wing inspection of the engine. This has allowed for an increase in service life of engine parts. Overall, the best way to prevent the defects of concern is through processing improvements and tight controls. However, even with an improved process, non-destructive testing will still be needed as a safety assurance to avoid the high impact of defects in jet engines. So the bottom line is the motivation for process improvement research ultimately comes from the manufacturer of the ingots who want to save money by reducing the amount of material that is rejected when it is inspected by the buyer.

As the demand for larger ingots has increased, so have the sizes of VAR furnaces. Since the arc is the primary source of heat in a VAR, an even distribution of the arc position versus time is becoming more important. Industry standard instrumentation provides a good assessment of the stability of the arc region but there is not a commercially available measurement system capable of detecting the spatial and temporal distribution of the arc during operation. Arc distribution has been shown to be related to conditions favoring defect formation, with ideal conditions being that of a diffuse arc.[1] This basically means the arc distributes evenly across the ingot surface at a time averaged level, leading to a quasi steady and uniform heat input to the surface. Figure 3 demonstrates that the prevailing arc distribution yields a visual difference on the electrode tip.

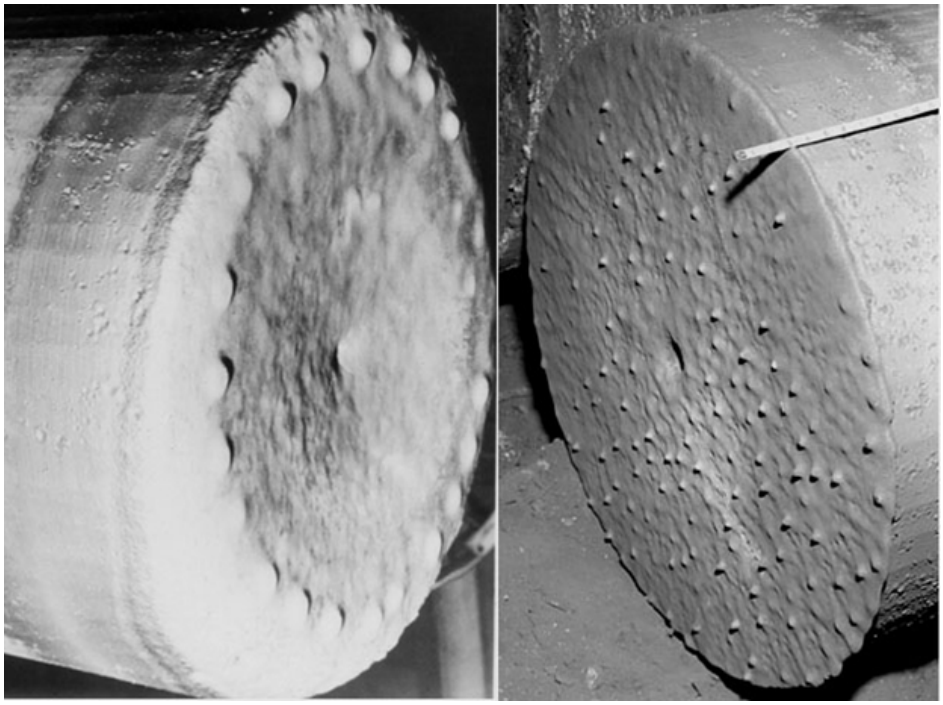

Figure 3: Electrode tips from aborted melts. The tip on the left resulted from a constricted arc condition whereas the tip on the right resulted from a diffuse arc condition (courtesy Zanner).

Assessing whether the VAR is operating with diffuse arc conditions by looking at the tip is not possible during the run, as the tip is not visible. Therefore, a real time, non-invasive measurement system that could assess the presence of this benchmark condition would be of value.

The effects that the arc can have on the molten material are categorized as either magnetic effects or thermal effects. The magnetic effect manifests as the Lorentz force, which is the force exerted on a charged particle in the presence of an electromagnetic field. This tends to cause a pattern of flow in the melt pool. It has been mathematically shown that the Lorentz force is a major contributor to the fluid dynamics in the arc region.[4] Therefore, a change in arc position causes a change in the fluid flow. The thermal effect requires more time to propagate into the ingot pool, on the order of the thermal diffusion speed. So variations of arc distribution over a time period will modify the shape of the molten pool in the ingot with the deepest part corresponding to the location where the arc is most concentrated. Also, fluid flow in the molten pool is driven by thermal convective forces so a change in arc position will change the fluid flow.

These thermal and magnetic effects of the arc can be implicated to some degree in most defects found in VAR produced ingots. Defects in these ingots can generally said to be solidification related or inclusion related. Solidification related defects form as the material is transitioning from a liquid to a solid. Inclusion defects come from unwanted material getting into the material and remaining intact.

Macrosegregation solidification defects in ingots are largely a function of processing. The defects form as bands or spots in the material. Spot solidification defects are called freckles or white spots with the former being associated with elevated levels of an alloying element, and the latter being associated with depleted levels of an alloying element. For instance, a nickel alloy freckle defect might be rich in niobium (strength adding alloy element) while a white spot defect would have low amounts of niobium. It has generally been observed in VAR operation that higher melting rates are more likely to cause freckles and lower melting rates cause white

spots.[5] So production practices find a middle ground, and this becomes the target melting rate.

The basic mechanism for the formation of freckle defects is best described by density inversion theory.[6] Gravity and thermal gradients at the bottom of the pool play important roles in their creation. It has been found that abrupt changes in the mushy zone likely contribute to the initiation for freckle formation. Changes in the mushy zone shape are a potential thermal effect of the arc, so the arc distribution is important in preventing freckles.

White spot defects can be found in various locations and with varying severity; most likely forming from multiple sources. For example, the defect could be caused by un-melted dendrites falling off the electrode into the melt pool, or by localized increase or decrease in the solidification rate in a manner similar to freckles. It is believed that many white spots in the interior of the ingot are associated with selective melting away of the ingot shelf. The shelf is the region near the top of the ingot that remains in contact with the crucible, as the remainder of the ingot pulls away from the crucible due to shrinkage during cooling. The best indication for this source is that white spots have been shown to specifically exist at a distance of around 12mm from the edge of the ingot.[7] The arc has a large thermal effect on the shelf because of its proximity, so arc behavior can again be implicated as playing an important role in the nucleation of this defect.

When ingot slices are etched a banded structure is revealed which appears to show the shape of the pool contour during the melt. In nickel super alloy these bands are characterized by alternating bands containing excessive and depleted amounts of the alloy element niobium. The cause is not well understood but it is thought that the Lorentz force and resulting fluid flow plays a significant role in the formation of the bands. Additionally, it is thought that the bands result from increased grain nucleation at the mushy zone front caused by macroscopic heat flux.[8,9] The thermal effect of the arc in shaping the pool shape can again be implicated as a source for the defect.

Inclusion defects can come from the source electrode material. It has been established that transfer of the metal from the electrode to the melt pool is largely a

bulk type process. This is important because it means non-metallic inclusions could be transferred to the ingot and not vaporized and removed via the vacuum. The arc plays an important role in metal transfer, both in suppressing and encouraging the formation of metal drops. A specially designed experimental VAR furnace with side viewing ports was constructed for high speed photography of the electrode gap region at the Sandia National Laboratory in the late 1970s. When molten material bridges the gap, a surge in current (drip short) temporarily extinguishes the arc. Interestingly, the research has shown that the arc actually re-ignites elsewhere before the rupture of the metallic bridge and the transfer of the metal to the ingot pool.[10]

The arc also interacts with the metal transfer (the arc consists of cathode spots as will be discussed in the next section) and the impulses from cathode spots actually slightly depress the surface of the pool. Also, the action of the arc causes a magnetic pinch which releases the drop into the ingot melt pool. The geometry of transfer of metal from the electrode to the ingot was found to be dependent on arc lengths. Ultimately, an electrode gap length control scheme was developed based on the highly linear correlation between drip short period and gap length measured in the videos.[11]

Ingots formed in a VAR will generally have a thin layer of material that extends from the shelf up the crucible wall. This is referred to as splatter, which is caused by the action of the arc to explosively eject some of the electrode's metal ions laterally to the crucible wall where it solidifies. The degree of splatter is directly related to the electrode gap length, essentially as a view factor effect. Splatter becomes a problem when it falls into the melt pool and re-melts. Without sufficient mixing in the pool the material can solidify as an inclusion in the ingot. This type of defect is referred to as fall-in. As discussed with white spots, the arc plays a significant role in the thermal behavior of the shelf wall due its proximity. Re-melt of the shelf can be detected by bore-site video measurements so a new measurement system is less useful for identifying process conditions that result in this defect.

Clearly, the distribution of the arc in a VAR furnace is an important operation parameter that could be monitored to assess the quality of the forming ingot. The monitoring system should be able to identify undesirable arc behavior characterized by

constant or varying constricted arc conditions which causes sharp or non-steady thermal and magneto hydro dynamic profiles in the melt pool. It has been shown with high speed cinematography of the arc region that a constricted arc can exist without leaving any evidence of its presence on current and voltage signatures.[12]

An output of the developed measurement system that would be useful to casting companies would be a real time plot of the distribution of energy into the surface of the melt pool. This could be shown in two dimensions, and as a time average. With this information traditional corrective measures could then be taken such as aborting the melt, varying the current, or varying the electrode position. Ultimately, an arc location measurement system would be even more valuable if coupled with magnetic control of arc location. Two United States patents exist for steering a furnace arc using externally applied magnetic fields.[13,14]

The cause of constricted arc conditions has also been studied. Confined arc conditions can be caused by the presence of slag on the surface, the presence of certain gases in the ambient, excessive gap lengths, and the presence of non symmetric magnetic fields.[1] Much of the knowledge on arc distributions in industry is based on examining electrode tips from aborted melts. Generally, the results show axisymmetric distributions with the tip being either being slightly concave or slightly convex.

Another useful application of an arc location measurement system would be in providing information to improve VAR solidification models. Significant work in the area of computational modeling of the process has been undertaken over the last 10 years. These models require energy inputs that currently require assumptions on the distribution of the arc. Knowledge of real distributions of the arc during VAR operations, or more specifically the spatial and temporal current densities in the furnace, will therefore provide an improvement to the modeling efforts.

Magnetic stirring coils are already being used on the outside of some large VARs, especially in the Titanium industry. Magnetic stirring coils are believed to help with the distribution of the arc, and also help confine the arc and prevent side-wall arcing. Typical operation might be running 15 amps through the coils while reversing direction of the current every 7.5 seconds. The use of stirring coils has been more

qualitative as opposed to quantitative, so this research could improve the understanding of the process. Indeed, small transverse magnetic fields as low as 5 to 10 gauss can steer the arc and cause a non-axially symmetric energy distribution.[15]

Knowledge of how vacuum arcs behave is critical to the VAR process. The next section details what is known about arcs in a VAR furnace, and how a measurement system based on magnetic flux density measurements could characterize arc behavior.

Vacuum Arc Behavior

A vacuum arc refers to an electrical discharge between a cathode and an anode at pressures low enough that the conduction path is sustained by vaporization and ionization of the electrode rather than the ambient gas. The ionized particles constitute the metal vapor plasma which exists between the cathode and anode. In a VAR the electrode is the cathode (V-) and the ingot pool is the anode (V+), so electrons flow from the electrode to the melt pool. VAR is not specifically directional though, in that it would still operate if the polarity was reversed.

The classical model for the behavior of metal vapor plasma arcs are based on small scale, short duration arcs in laboratory experiments. The electrical discharge emanates from cathode spots which are small and mobile zones which eject ions and material from the electrode. For copper, it was found that a given cathode spot can only carry a maximum current of about 100 Amps.[16] If the total current exceeds this, multiple cathode spots form with each spot carrying less than the maximum allowable current.

The Typical VAR electrode, which conducts thousands of Amps, will therefore have multiple cathode spots. From a measurement stand point it is important to know whether these individual spots cluster and remain collinear which, from a distance, would look like a single arc. Or the individual spots might behave individually, creating the impression at a distance of multiple arcs.

Attempts have been made to study VAR arc behavior in specially designed furnaces that have view ports to allow direct visualization of the electrode gap. High speed photography then captures the action. Research in this area was done at the NETL site, in Albany in the 1980s. It was found that arcs could move toward the edges at speeds up to 900 m/s.[17] Experiments were performed in a large furnace having AC power, and non-consumable electrodes, so it's unclear whether this speed of movement could be expected in a DC VAR furnace.

Specific to VAR arcs, important research has been performed by Dr. Frank Zanner and others at the Sandia National Laboratory using high speed cinematography to study the electrode gap region. This works gives insight into VAR arc motion. It was found that a cathode spot jumps on a microsecond scale to an adjacent position creating a sort of random position walk across the surface. Figure 4 shows an image of the electrode gap region inside a VAR furnace.

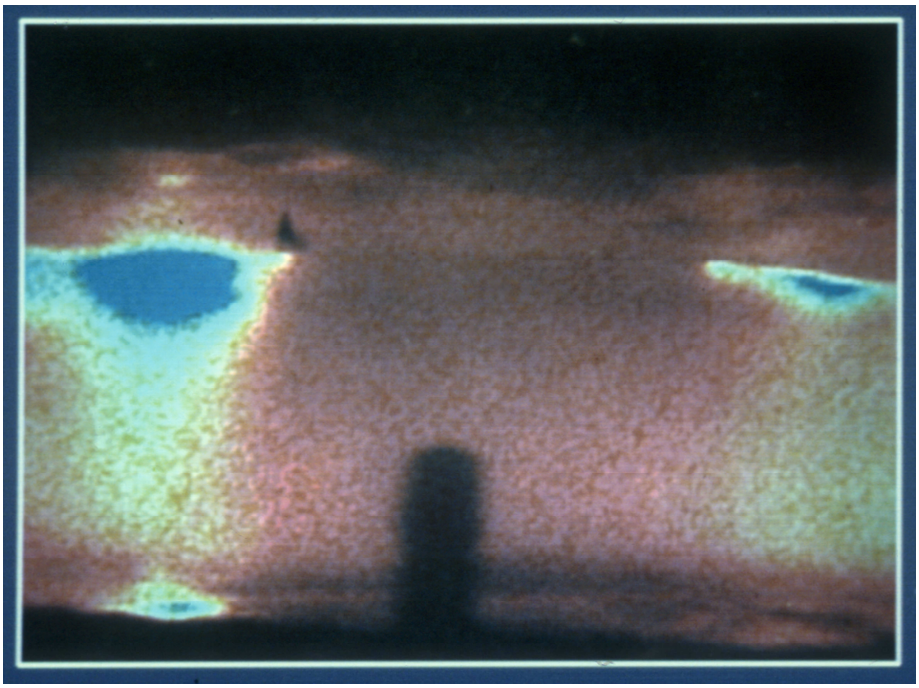

Figure 4 : Enhanced image of the electrode gap region in a VAR operating at 2.2kA. A 6mm diameter tungsten post is visible in the foreground. (Courtesy Zanner)

Cathode spots appear as blue light while the plasma can be seen as a diffuse background cloud covering the whole region. Although the position of an individual cathode spot was largely random, it was reported that there was a general trend for the spots to form near the center of the electrode and then move in the radial direction, crawling up the lateral surface before extinguishing. The time period for this was on the order of 10^{-3} seconds. Instead of the classical diffuse model, there seemed to be spatial relationships with a strong periodic component. Additionally, he observed behavior of cathode spots tending to move around in ill-defined clusters, separating and coalescing with retrograde motion. Overall, the ill-defined nature of the cathode spots made inferring current distribution from the video data ineffective as a means to estimate current distribution on the ingot face.[18] Also, the side port high speed cinematography method for visualizing the arc cannot be adapted to work on existing furnaces.

Non-intrusive, externally mounted sensors to characterize the arc region would be ideal. This can be realized by considering the arc as a current density source and utilizing the relationship between current density and a magnetic flux density which can be measured. The relationship is shown in equation 1, known as the Maxell-Ampere equation.

$$\nabla \times \vec{B} = \mu\left[\vec{J} + \frac{\partial \vec{D}}{\partial t}\right] \tag{1}$$

In this equation $\nabla \times \vec{B}$ is the curl of the magnetic flux density, μ is the permeability of the medium through which the field is diverging, $\vec{J}$ is the current density, and $\frac{\partial \vec{D}}{\partial t}$ is the rate of change of the electric field which is sometimes referred to as the displacement current. The terms are vectors. Permeability is a material property. Fortunately, the materials in and around the furnace all have a relative permeability of 1, meaning the permeability is the same as in vacuum. Therefore, the magnetic field diverges from the arc un-distorted.

In the ideal operation of a DC-powered VAR furnace, the current is held at a near constant value. Currents that are constant mean that the magnetic field is constant. This eliminates the rate of change term in the above equation leaving the Maxwell-Ampere as equation 2.

$$\nabla \times \vec{B} = \mu\left[\vec{J}\right] \tag{2}$$

Certainly fast transients in VAR operation could violate magneto-statics to some extent. Metal transfer drip shorts have been shown to last over a 0.0003 to 0.0205 second time scale.[19] These events take up 3 to 5 percent of the melting time. Still, using the magneto-static equation is a good starting point. Indeed, electrical processes changing in the 60Hz range can be solved using magneto-statics without introducing much error.[20] Additionally, the time scales of significance to the formation of defects are much slower, closer to the thermal diffusion speed. So the electromagnetic characteristics of interest can be said to be quasi static.

Hall Effect sensors can effectively measure the external magnetic fields and there are commercially available multi-axis Hall Effect sensors. The multi-axis sensor has two or three closely spaced, orthogonally oriented sensor elements that can be used to sense the direction of the magnetic flux in addition to the intensity of the magnetic flux. A sensor element works by passing a current across a conductor or semi-conductor and the Hall Effect causes this current to interact with the magnetic field of interest, displacing the flow of electrons. This electron displacement causes a voltage difference across the element that can be measured. The resulting voltage output of the sensor is a function of the magnetic field, the applied current, the area and thickness of the sensing element, and a material dependent property. Thus, signal conditioning can extract the desired quantity, which is the magnetic flux density, and the multi axis version allows a magnetic flux density vector to be calculated.

There have been previous published studies using multi-axis Hall Effect sensors to characterize VAR arc conditions by R.M. Ward in the U.K. [21] Indeed, his work provides the inspiration for conducting this study. His technique involved using

magneto static finite element modeling to solve for the magnetic flux density vector at a sensor's location for various single arc location simulations. The magnetic flux density simulation results were then compared to the measurements and a most likely arc position was determined via regression. The method he used involved an iteration weighting the determination to favor sensor predictions closest to the arc. He found an arc distribution favoring a region close to the edge of the electrode, with nearly no occurrence of the arc at exactly the very center of the electrode. Also, he found that there may actually be an ensemble arc motion at intermediate time scales. The ensemble motion was an arc distribution concentration that traveled around the furnace azimuthally with a time period of around 30 seconds. The formation of defects would certainly be encouraged by changing current density concentrations at these time scales.

It should be noted that the magnetic field external to the furnace results from not only the current moving through the arc, but also the current moving through the rest of the furnace. Indeed the small dimensions of the electrode gap mean that most of the magnetic field external to the furnace derives from current elsewhere in the furnace. So really measuring the external magnetic field is measuring the change in current conduction path in the rest of the furnace due to movement of the arc. Fortunately, the coaxial nature of many furnaces mean diffuse arc conditions will cause no net magnetic field outside the furnace, and so the measurement system can have a good signal to noise ratio if the signal is considered to be a variation from this condition.

Since the external magnetic field arises from current paths in the furnace, an understanding of how current moves through the furnace is necessary to design an effective measurement system. In addition to melt specific parameters that may be important such as heterogeneities in the electrode causing current path variations or variable contact between the ingot shelf and the crucible there are some general current path studies worth considering.

It is well known that the total power applied to a VAR furnace does not explain the melting rates observed. Specifically, there is a significant efficiency loss, in that

only 50 to 60 percent of the power goes to cathode heating. Zanner et al performed an energy balance on operation that considered the heat up time from operation start to melting point. Overall, he found approximately 20% of the current moved through the plasma in a non-classical sense in that the current was not part of an arc.[22]

In addition, attempts have been made to track the current movement from the electrode to the crucible by measuring the surface voltage profile on the crucible. It was found that only 63% of the total current appeared to travel through the ingot pool, with the remaining balance traveling directly from the electrode to the crucible.[23] This value was shown to not vary when the interior of the copper crucible was coated with Titanium Dioxide.

The use of external magnetic flux density sensors can allow for both monitoring of arc behavior in the electrode gap, and monitoring of the current profiles in the rest of the furnace. However, the fact that both signals exist in the measurement mean a deterministic arc tracking measurement system is only possible if assumptions are made regarding the current profiles. Overall, monitoring external magnetic fields has great potential for arc furnace control, as well as in improving the basic understanding of the process.

Methodology

The primary motivation of this research is to improve processing conditions in the largest of VARs. The VAR systems at NETL, Albany are relatively small, and so the relationship between arc distribution and defects could be much different than that of a large VAR. With small VARs available for testing, the research was best served by developing the measurement system, as opposed to performing crystallography or other metallographic techniques on the formed ingots, and then relating them to the time-history of the electro-magnetic fields. Therefore, the focus of this paper is on developing the measurements system, rather than focusing on studying the relationship to preventing the formation of defects in ingots cast in VARs.

The work done toward this thesis can be summarized into two major tasks. First, the VAR furnace data acquisition system was designed and installed. Second, an analysis system was implemented to use the data acquisition system to investigate arc behavior. Although the first step took quite a bit of engineering and troubleshooting, those details are left out for the sake of brevity. It should also be noted that this is the first undertaking of magnetic field monitoring of arc furnaces at NETL, so this research serves as a foundation for future study.

Prior to investigating dynamic arc behavior, controlled and static experiments were performed to validate the developed analysis technique. These involved passing a known current through a conductor at a known location, and seeing if the analysis system could correctly locate the conductor using only the current and magnetic field measurements.

As a general approach, it was desired to not make any assumptions on what the arc distribution should look like, and to avoid using correlations as much as possible. However, as an analysis starting point it was assumed that there is a single arc. Starting this way is logical because this is the simplest approach to investigating VAR arc behavior.

The following list summarizes the types of analysis used in this study to characterize arc behavior.

1. Basic Signal Analysis
    a. Magnetic flux density and current data in the time domain
    b. Current and magnetic flux density in the frequency domain using the Fast Fourier Transform (FFT) method

2. Finite Element Analysis (FEA)
    a. Furnace geometry and various arc positions numerically simulated as finite element models
    b. Simulated FEA data is fit to an equation to arrive at a deterministic, real time capable, and sensor independent arc location solution
    c. Various types of signal simulation are input into the analysis algorithm

3. Supporting Evidence Analysis
    a. Post melt surface photographs of the ingot and stinger
    b. Correlations to the simultaneous bore-site videos acquired during the melts

Distinctly unique to this thesis compared to the previously published work by Ward is items 2b and 2c. Indeed it is shown that a single sensor can deterministically locate an arc. Additionally, by treating data from separate sensors as independent quantities, additional information can be inferred on the behavior of VAR arcs. Also unique to this study is the use of the controlled, static tests to validate the analysis technique.

VAR Instrumentation Set-up

There are two research VARS at NETL Albany, which were originally built in the 1940's and 1950's. The furnaces can be seen Figure 5, the chamber closest to the camera is referred to as the coaxial furnace, and the other system is referred to as the non-coaxial furnace.

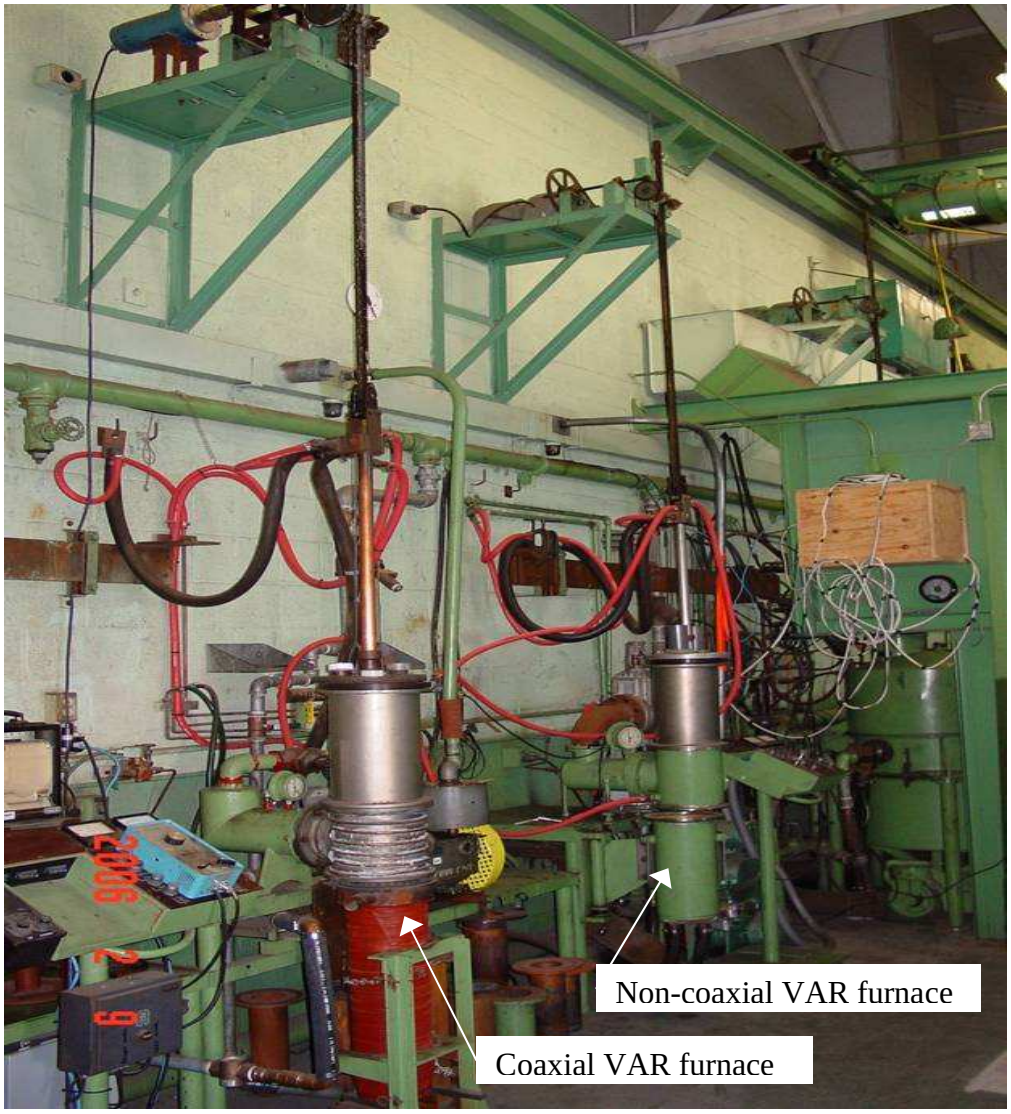

Figure 5 : Experimental VAR furnaces at NETL, Albany

The furnaces are capable of holding crucibles up to 6 inches in diameter and 20 inches in length. A bank of DC welders provides power, and is capable of up to 30,000Amps and 100Volts. Typical operation for these furnaces is in the 1200 to 4000Amps range at 20 to 30 Volts.

The furnaces were already equipped with a large shunt resistor in series with the furnace to measure the current, and probes to measure the voltage drop across the furnace. These are located near the power supplies, which are not shown in the picture. Two analog cameras are attached to view ports on top of the furnace immediately before operation. The cameras view the melt pool from above and on opposite sides of the electrode. During a melt, the ingot surface moves closer to the cameras and more light reaches the cameras. So the aperture and focus of the cameras are continuously manually adjusted during the melt. Artificial lighting is not required, the light emitted by the arc and drip short explosions are more than bright enough and indeed neutral density filters are utilized to reduce the intensity of light reaching the camera.

The signals from all of the instrumentation are routed to the operator's location, which is behind a brick wall. The brick wall acts as a blast shield to protect personnel, in case of crucible wall failure, when melting highly reactive metals such as Titanium.

The challenge for adding the data acquisition system was to add the multi-axis Hall Effect sensors and then to adapt all of the existing instrumentation to a computer based data acquisition system.

A National Instruments data acquisition system was selected, capable of digitizing 32 analog inputs, 2 analog video signals, and having a maximum 100 MHz transfer rate between the converters and the computer's hard disk. Figure 6 shows the set-up.

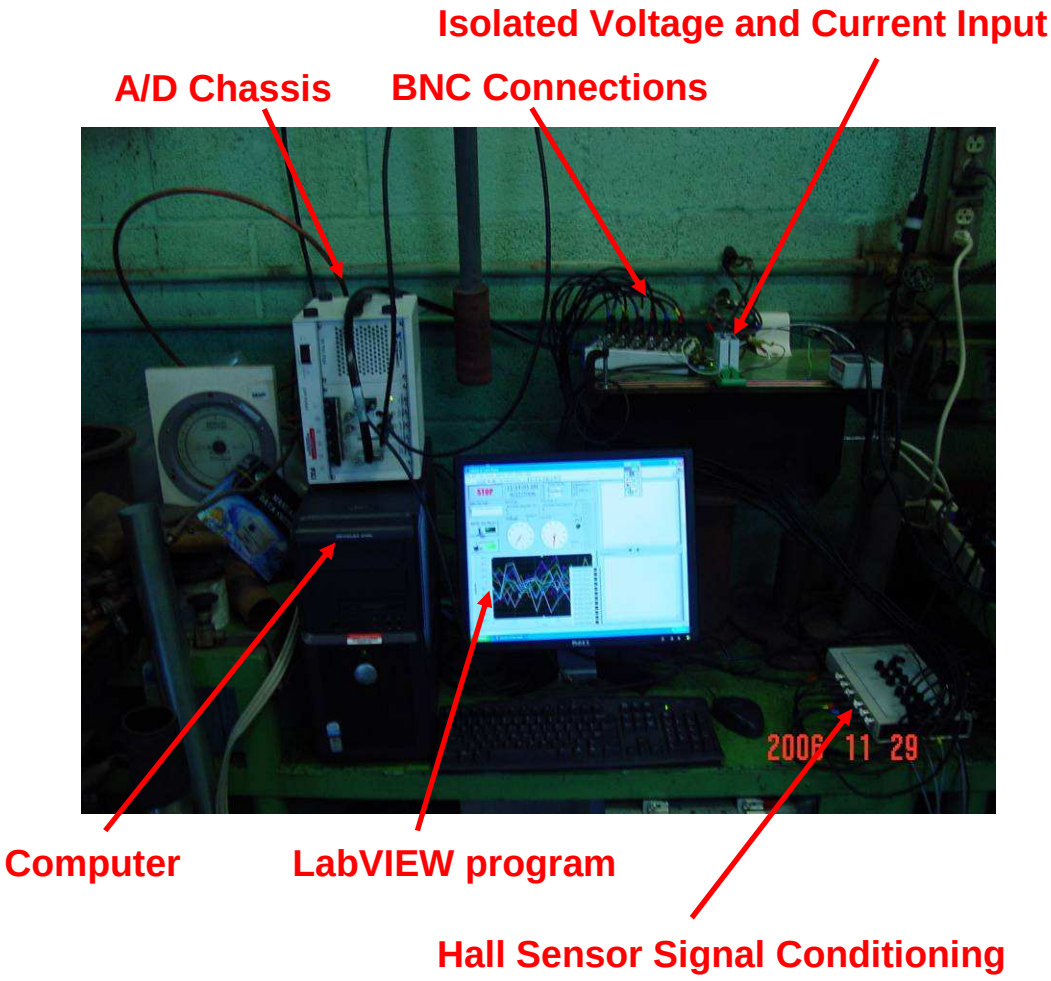

Figure 6 : Data acquisition set-up

The acquisition program was written using LabVIEW. Due to the high bandwidth needs for the 2 video channels, low level programming and data buffers had to be used. Timing between the analog data channels and video was accomplished using software timing.

Voltage and current acquisition used front end isolated signal conditioning units from DataForth so that the data acquisition system would be electrically isolated from the current path in the furnace. This improves the overall signal to noise ratio for the data acquisition. Table 1 summarizes the specifications for the measurements.

Table 1 : Instrumentation Specifications

	Magnetic flux density	**Current**	**Voltage**	**Images**
Description:	Four 3-axis hall effect sensors	Isolated op-amp	Isolated op-amp	A/D video converter
Channels:	12	1	1	2
Range:	+/- 500 gauss	+/- 10,000 A	+/- 100 V	1V white ref. level max.
Resolution:	0.01 gauss	1 A	3mV	24-bit color
Bandwidth:	20 kHz	10 kHz	10 kHz	30 Hz

The Hall Effect sensors transform the magnetic flux density into a readable voltage. Each of the four Hall Effect sensors has three separate 0.2” square sensing elements configured at 90 degrees apart. The elements are housed at the end of an aluminum square tube measuring 0.25” x 0.25”. The response to the magnetic flux density is perpendicular to the labeled axis and the voltage output of the signal conditioning box is linearly proportional to the applied magnetic flux at 1mV/gauss. Assuming the sensor is placed in a region where the gradient of the magnetic flux is minimal over the dimensions of the sensor, the data for the three elements can be transformed into a vector containing a direction and magnitude of the magnetic flux density at a point. Thus, a magnetic flux density vector is determined at four separate points outside the furnace.

It is important to note that the sensors do not respond to the electric field. So, a change in voltage in the furnace will not have an effect on the sensor. The sensors respond to the earth’s magnetic field, which is fairly constant at about 0.5 gauss. So, the sensors are electronically zeroed once in place on the outside of the furnace.

The Hall Effect sensors were directly attached to the outside of the coaxial VAR furnace. Figure 7 shows the set-up coordinate system. The sensors were placed at a z-direction location on the furnace that corresponded to approximately half way up the final ingot's height. This varied for each experiment, as can be seen in the next section.

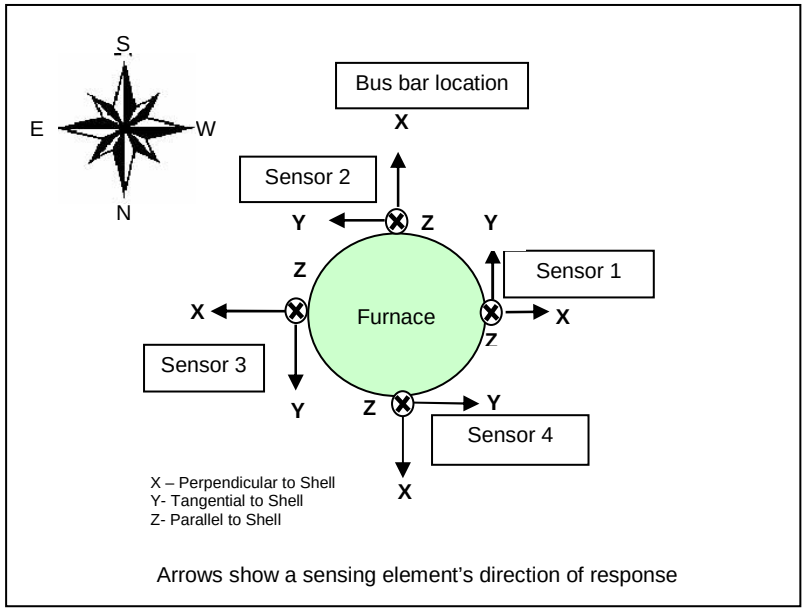

Figure 7 : The sensor set-up coordinate system

The set-up resembles a cylindrical coordinate system. The relationship between current and the direction of the resulting magnetic field can be assessed using the right hand rule with the thumb pointed toward the minus, and the magnetic field curving around with the curl of the fingers. So, in this set-up, the y-axis on each sensor primarily responds to current moving in the axial direction. The x-axis responds to current moving azimuthally, and the z-axis primarily responds to current moving in the radial direction. However, of particular interest is the change in position of an arc which is an axial current, and this will cause both the x-axis and y-axis to show a

change in the magnetic flux density. To a lesser extent the z-direction current will also change because radial current will increase on the side closest to the arc.

In general, current takes the path of least resistance. So changing the current path in one part of the VAR changes the current path in the rest of the VAR, which is easy to understand but difficult to analytically solve in a complicated geometry. To solve for the current distribution in a VAR furnace, finite element modeling was used.

Finite Element Analysis

COMSOL Multiphysics, a general finite element analysis (FEA) software package, is utilized. COMSOL solves problems based on partial differential equations (PDEs). When solving the PDEs, COMSOL Multiphysics uses the proven finite element method (FEM).[24] Even though VAR furnace geometry is often designed to be axisymmetric, the modeling is done in 3-D to be able to account for off centered arcs.

First the geometry of the furnace and the experiment is drawn. For the melts, a modeled ingot height is used that corresponds to about half the final height of the formed ingot. This also meant the modeled electrode gap was nearly lined up with the sensor's axial location. The presence of a single arc is modeled, so separate models are created for each arc location simulation.

Each individual component in the furnace is considered to be a subdomain with defined material properties. The relevant properties are electrical conductivity and relative permeability. As already mentioned, the furnace contains material with a relative permeability of near 1. The conductivity of the arc was set to a value similar to graphite at 10,000 S/m. This value has little effect on the solution because the surrounding area was modeled as space with extremely low conductivity, forcing all the current through the arc. In reality, previous studies indicate that there is diffuse conduction of some of the current through this space by the plasma, as previously discussed. Neglecting this effect could result in an attenuation of the predicted arc motions.

Boundary conditions are then set-up. The bus bar connecting power to the crucible is defined as a current input to the model and the electrode ram is set to ground, or zero volts. The entire model region has to be surrounded by a boundary which is defined as electric and magnetic insulation. This basically sets the values of the magnetic and electric field at these boundaries to zero so that the PDEs can be solved. As long as the space is big enough, the error in doing this is minimized. Interior boundaries are set-up as continuity so these boundaries have no effect on the calculations.

The entire model is then meshed to create the discrete finite elements. In the cross section through the arc and sensors, a finer mesh region is used to reduce mesh size related errors. Additionally, the sensors are modeled with an even finer mesh. Figure 8 shows the meshed model, as described.

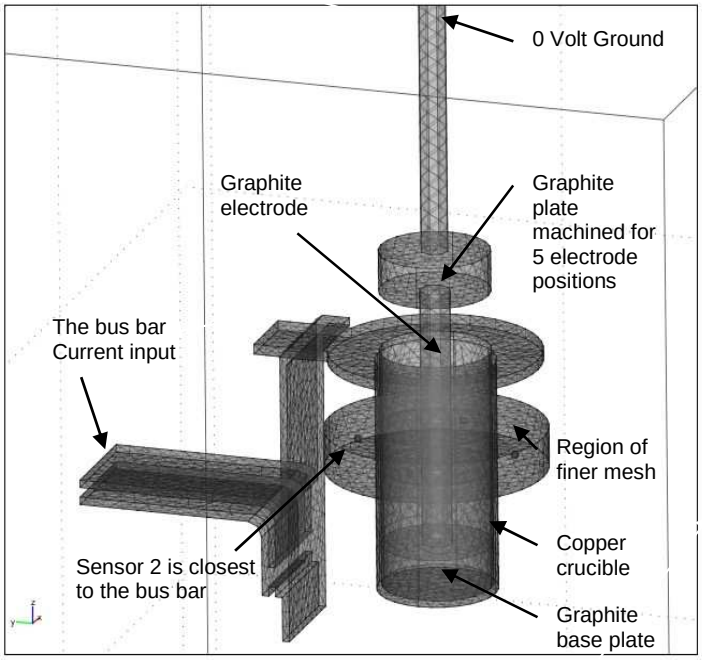

Figure 8 : The finite element model of the coaxial VAR. Shown is the static center test.

Thermal or magneto-hydro-dynamic processes are not modeled in the finite element analysis. These processes are important to VAR operation, but can be neglected in the model because the processes will not have an arc location independent effect on the external magnetic flux density.

Each arc location simulation is modeled separately, at a fixed position with a static current. Therefore, static electromagnetic equations apply. The solution is considered to be coupled in that electrostatics and magnetostatics are solved separately in that order. First, the model calculates the electrostatics using equation 3.

$$-\nabla \cdot (\sigma \nabla V - J^e) = 0 \tag{3}$$

The σ term is the electrical conductivity (S/m), J^e is the externally generated current density vector model input (A/m^2), and V is the electric scalar potential vector (Volts). For the given conditions, this essentially solves for the current path through the furnace. The electric scalar potential solution then becomes input into the magnetostatic solution using equation 4.

$$\nabla \times \left(\mu_0^{-1} \mu_r^{-1} \nabla \times A\right) + \sigma \nabla V = J^e \tag{4}$$

The μ_0 term is the permittivity in vacuum (8.854*10^{-12} Farad/m), μ_r is the relative permeability (dimensionless), and A is solved for. A is the magnetic vector potential (Weber/m). The Magnetic flux density vector is directly related to the curl of the magnetic vector potential, as seen in equation 5.

$$B = \nabla \times A \tag{5}$$

B is the magnetic flux density vector (Weber/m^2 or Teslas), and 1 Tesla is equivalent to 10^4 gauss. COMSOL is set-up to automatically choose the most efficient stationary solver to solve the equations for the finite elements in the model.

Next, simulation results can be plotted. Some of these results are now presented. Figure 9 shows streamlines of the current from the bus bar to the crucible to the graphite electrode assembly for the static center test. As mentioned, the idea for static tests was to see if the developed analysis method could correctly locate the position of the graphite electrode from magnetic and current measurements. No arcing or melting took place.

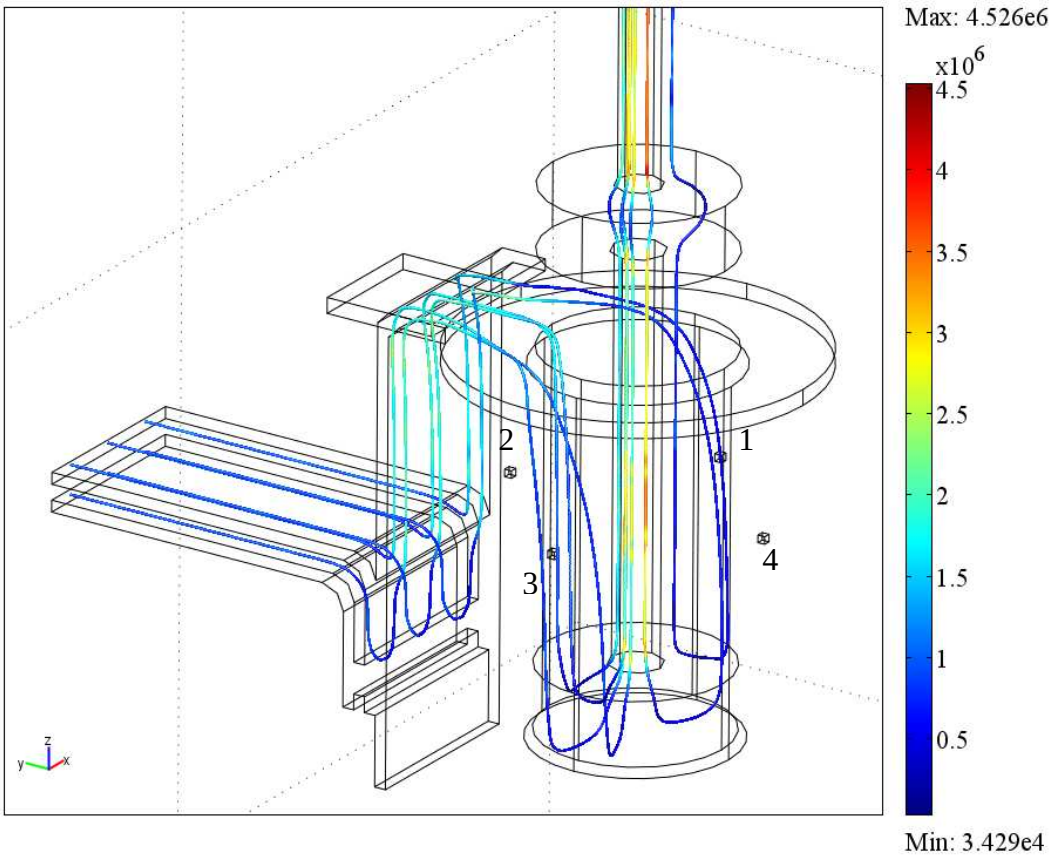

Figure 9 : FEA of current path for static center test. Streamlines are colored by current density (A/m^2). Input current was 4645 A.

Not shown in the figure is the furnace shell, so the sensors appear to be floating in mid-air. The sensors appear as cubes, and are labeled by number. Figure 10 shows a slice of the magnetic flux density through a plane containing the sensors.

Also, the magneto static model shows a linear response of magnetic flux density versus current, as expected.

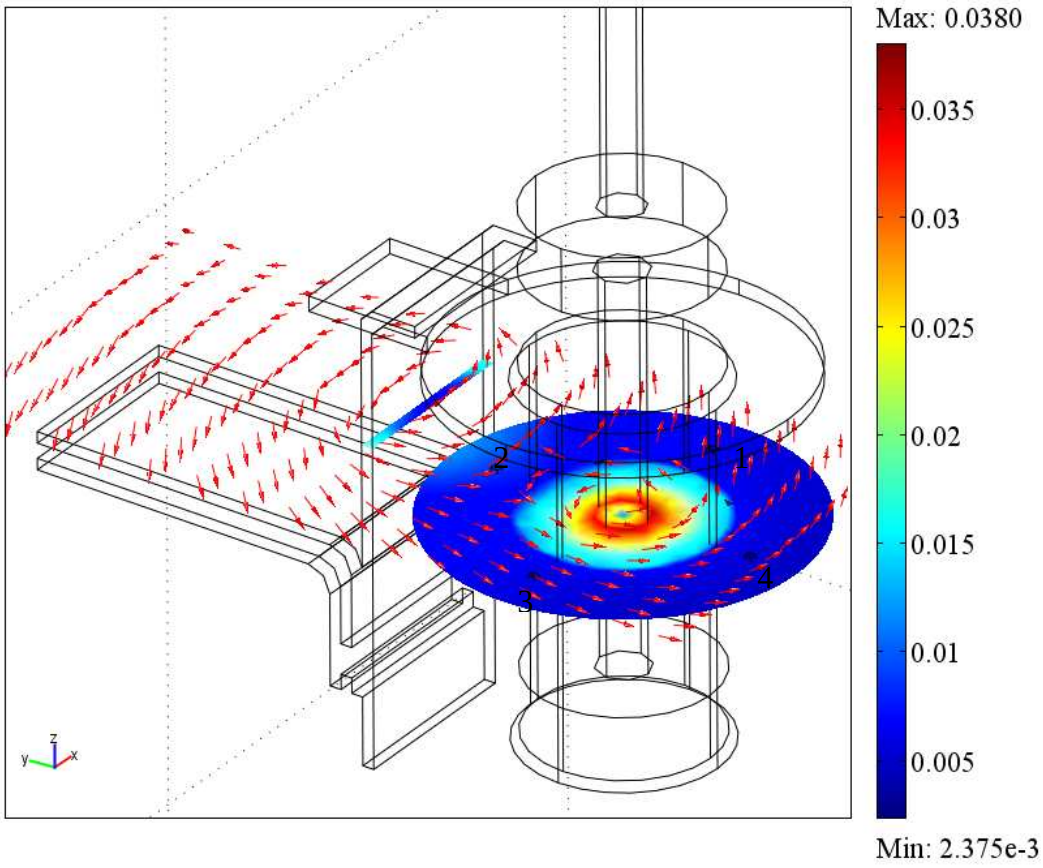

Figure 10 : FEA of magnetic flux density for static center test. Colored slice indicates the normalized magnetic flux density (T) and arrows show the normalized direction.

It can be seen that the largest magnetic flux density is inside the furnace, with a maximum of 380 Gauss. This compares to about 29 gauss at the sensor 4 position, and 78 Gauss at sensor 2 positions. This drop off is due to the divergent nature of the magnetic flux density, and because of the canceling of the external magnetic fluxes due to the coaxial set-up. Still, the furnace can hardly be called coaxial, since a truly coaxial furnace would result in a zero external magnetic flux density at the sensors'

locations. Clearly, the cause is the non-axisymmetric bus bar in close proximity to the furnace.

Figure 11 shows the simulation for the same current when the electrode is displaced south 2 inches, toward sensor 2.

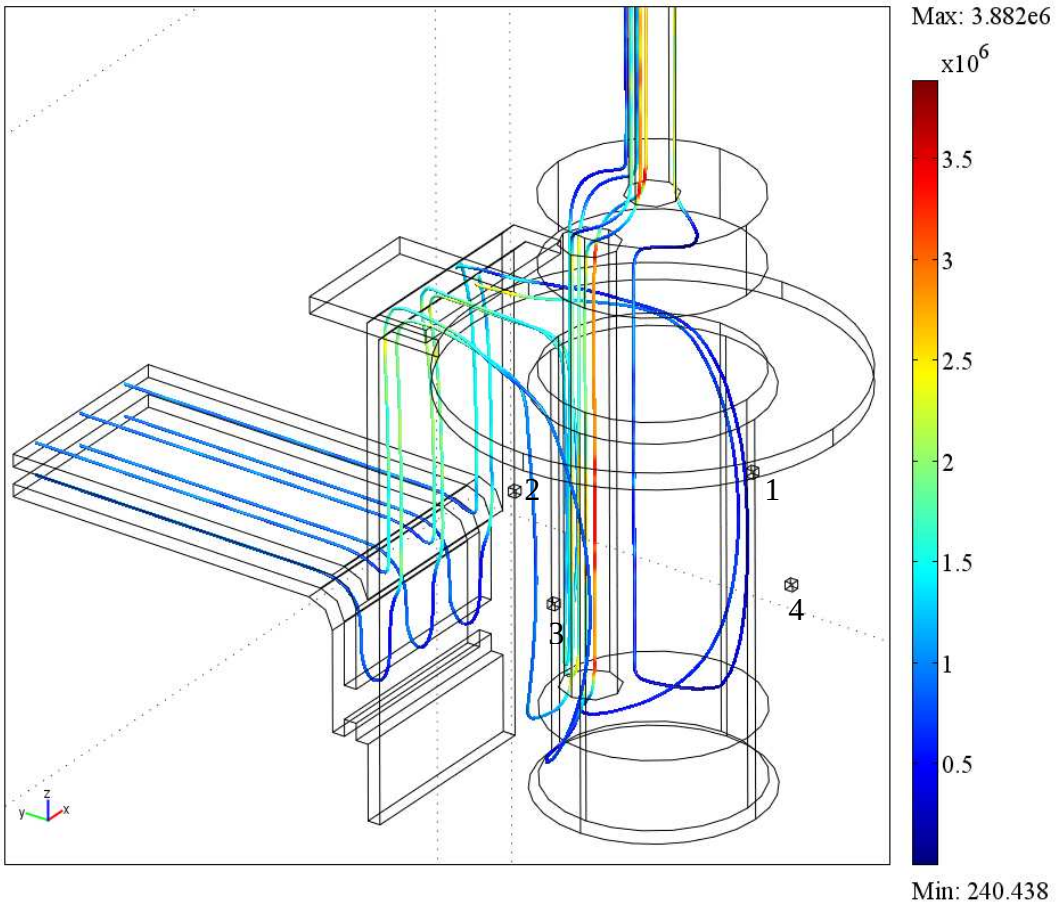

Figure 11 : FEA of current path for static south test. Streamlines are colored by current density (A/m^2). Input current was 4600 A.

As expected, the current favors the side of the crucible that is closest to the electrode. The main purpose of showing the streamline plots is to visualize the set-up

and current paths for different experiments. Figure 12 shows the magnetic flux density for the static south test.

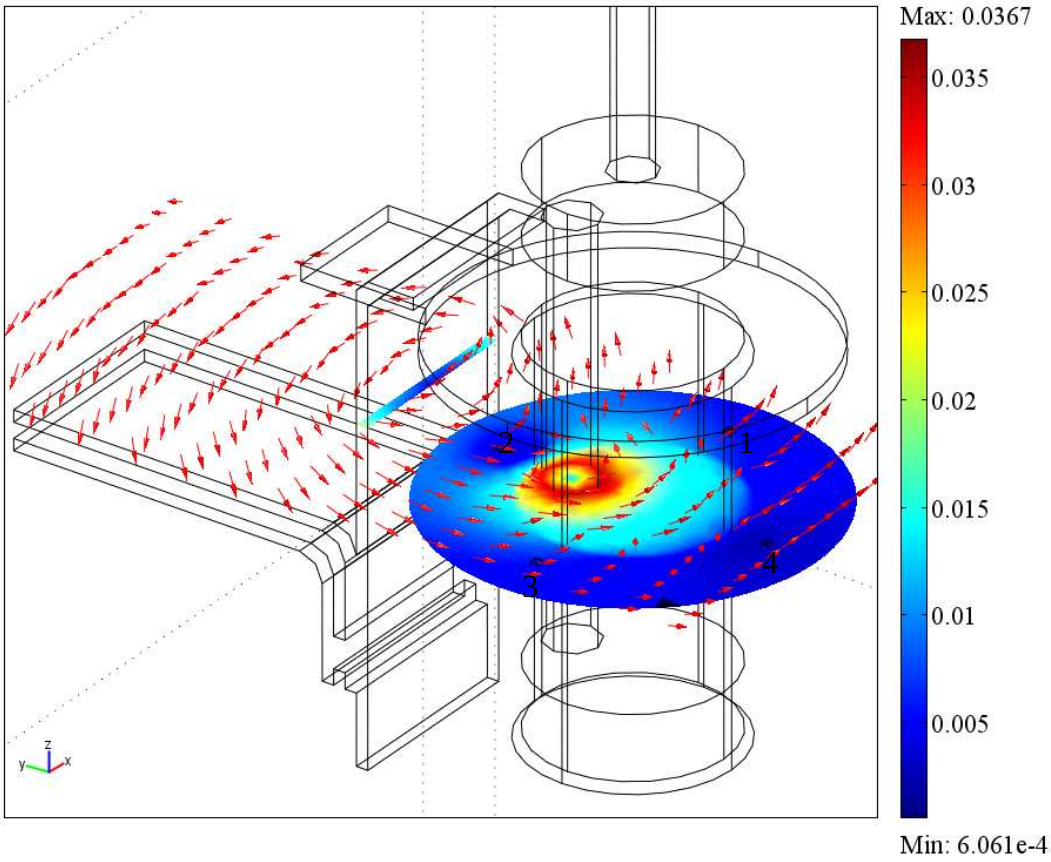

Figure 12 : FEA of magnetic flux density for static south test. Colored slice indicates the normalized magnetic flux density (T) and arrows show the normalized direction.

It can be seen that moving the electrode does not have a great effect on the maximum magnetic flux inside the furnace, and that the maximum moves with the electrode. Also, it can be seen that sensor 1's location is in an area with a considerable amount of flux in the z-direction. Finally, sensor 2 is in a location where there is both a large gradient in terms of magnitude and direction of the magnetic flux. This means there is likely to be more error in the results from sensor 2 because of the uncertainty in the actual position of the sensor with respect to the rest of the furnace.

Figure 13 shows one of the FEA simulations for the 4-inch In-625 melt. The location of the sensors and center simulated arc position can be clearly seen.

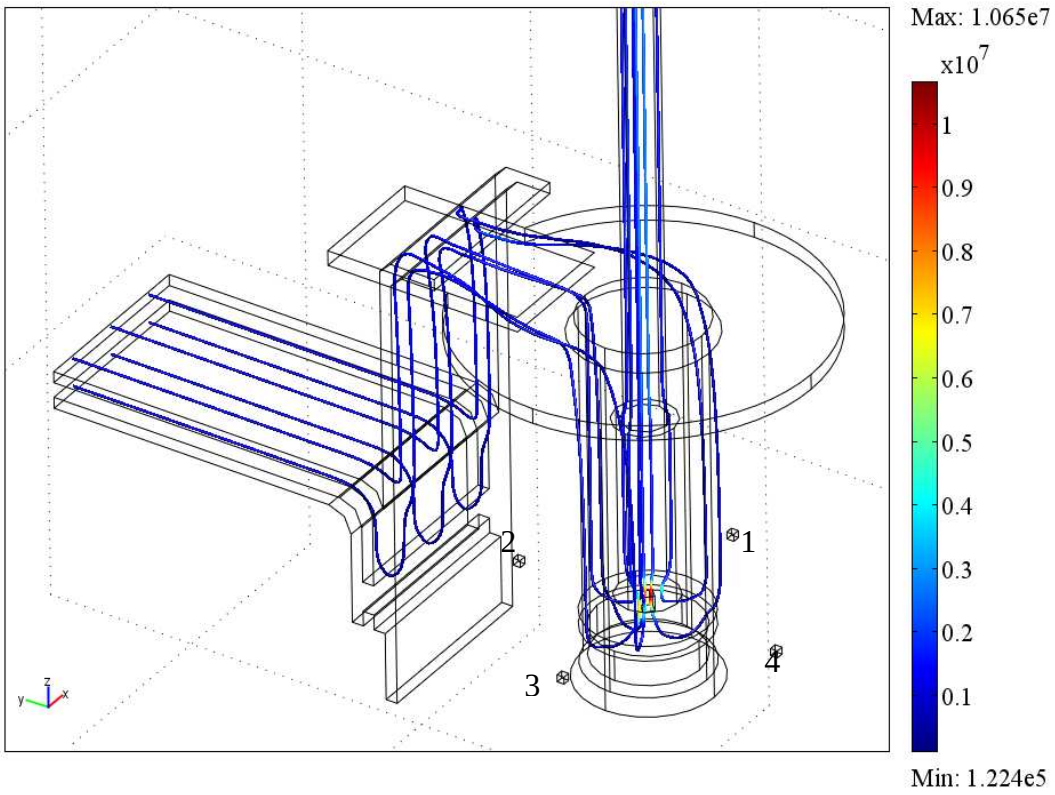

Figure 13 : FEA of current path for 4-inch In-625 melt with centered arc. Streamlines are colored by current density (A/m^2). Input current was 3000 A.

Figure 14, on the following page, shows the resulting magnetic flux density for a plane through the sensors.

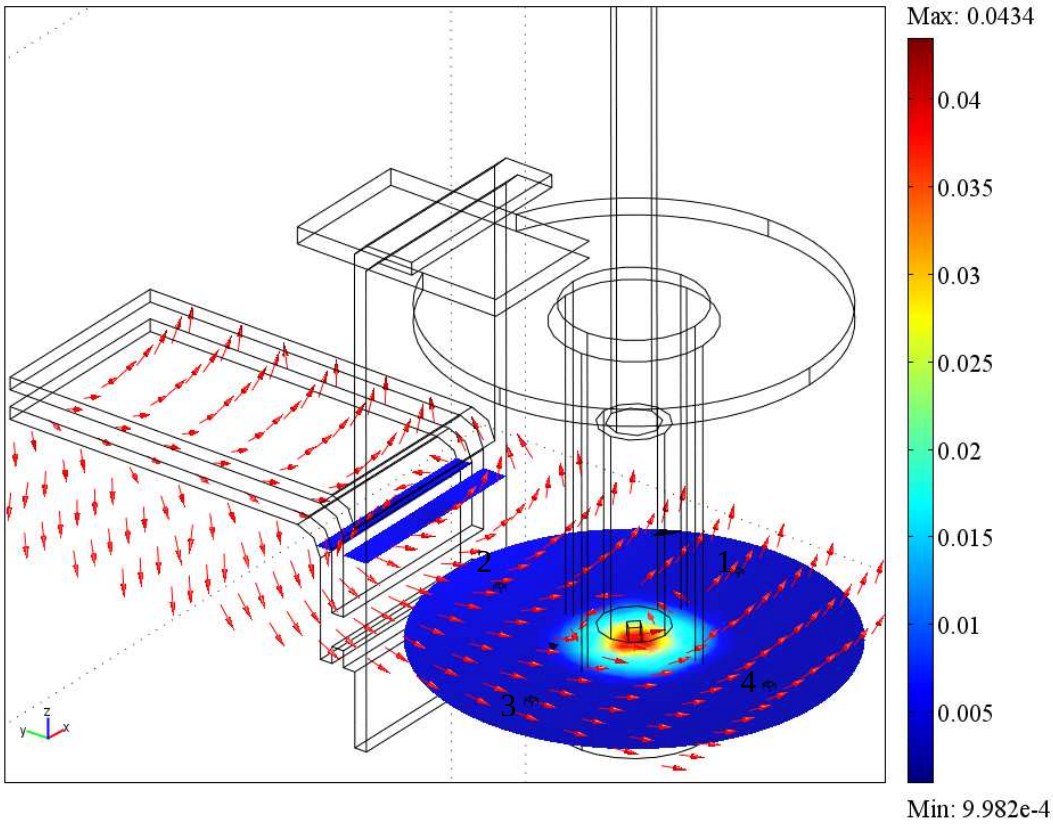

Figure 14 : FEA of magnetic flux density for 4-inch In-625 melt with centered arc. Colored slice indicates the normalized magnetic flux density (T) and arrows show the normalized direction.

Figure 15, on the following page, shows one of the simulations for the 6-inch SS 316 test. This used the same crucible as used in the static tests.

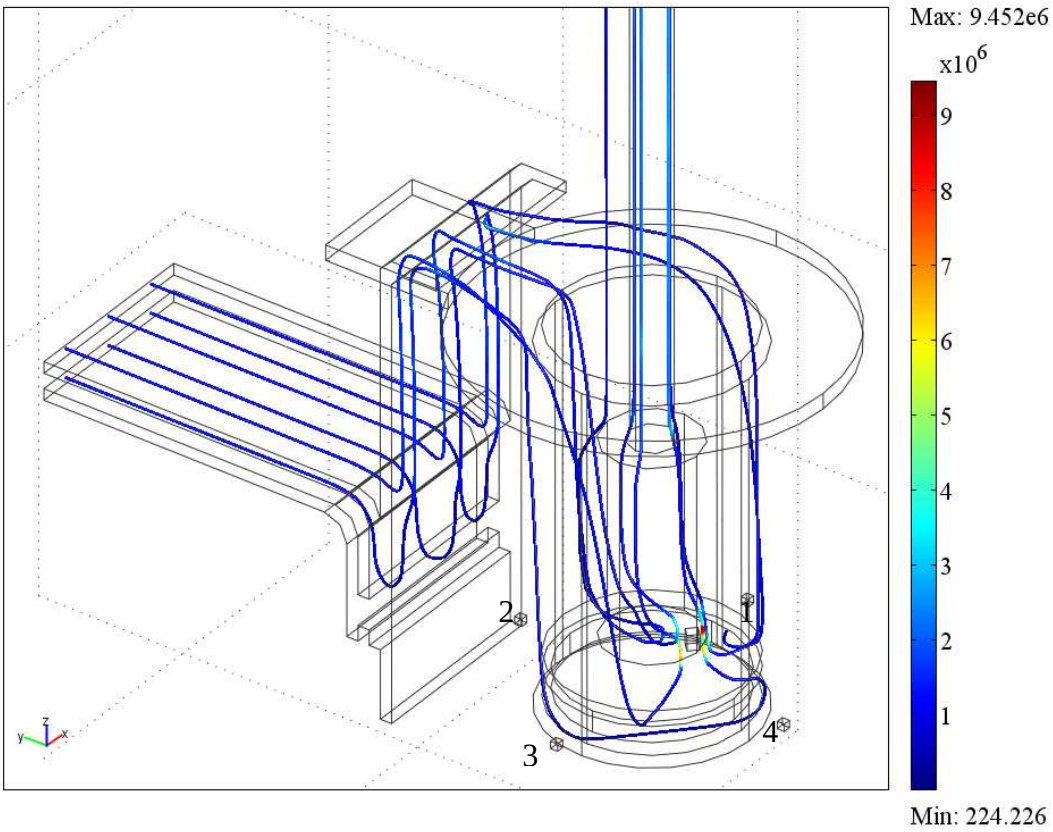

Figure 15 : FEA of current path for 6-inch SS 316 melt with offset arc. Streamlines are colored by current density (A/m^2). Input current was 4000 A.

It can be seen that the level of melt was very low, so the sensors were placed near the bottom of the crucible. Figure 16, on the following page, shows the resulting magnetic flux density for a plane through the sensors.

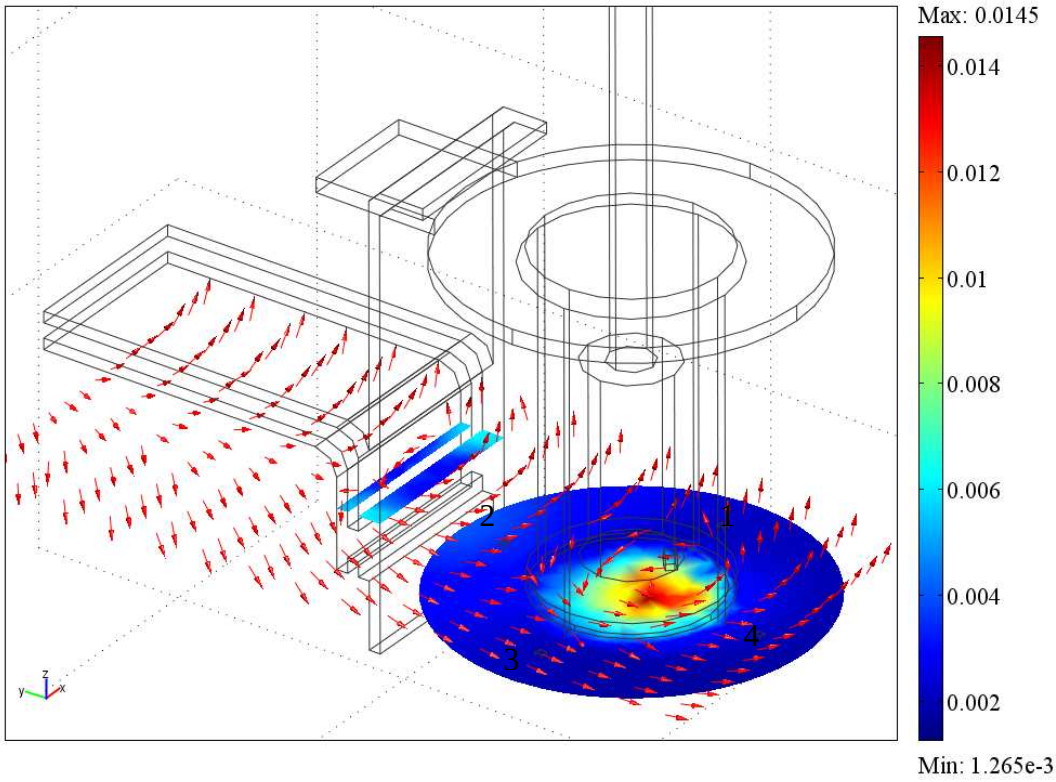

Figure 16 : FEA of magnetic flux density for 6-inch SS 316 melt with offset arc. Colored slice indicates the normalized magnetic flux density (T) and arrows show the normalized direction.

In this case it can be seen that the sensors were located slightly below the arc for the simulation. This is why the area showing the maximum is not where the arc is, but rather offset toward the middle. This shows that the axial location of the arc has a large effect on the magnetic flux density at a point in a cross-sectional plane inside the furnace. The effect of this is minimal outside the furnace where the sensors are located.

Figure 17, on the following page, shows an FEA simulation for the 6-inch In 625 melt. This used the same crucible as the previous melt, but different sensor locations, and a different simulated ingot height. This was because more material was melted.

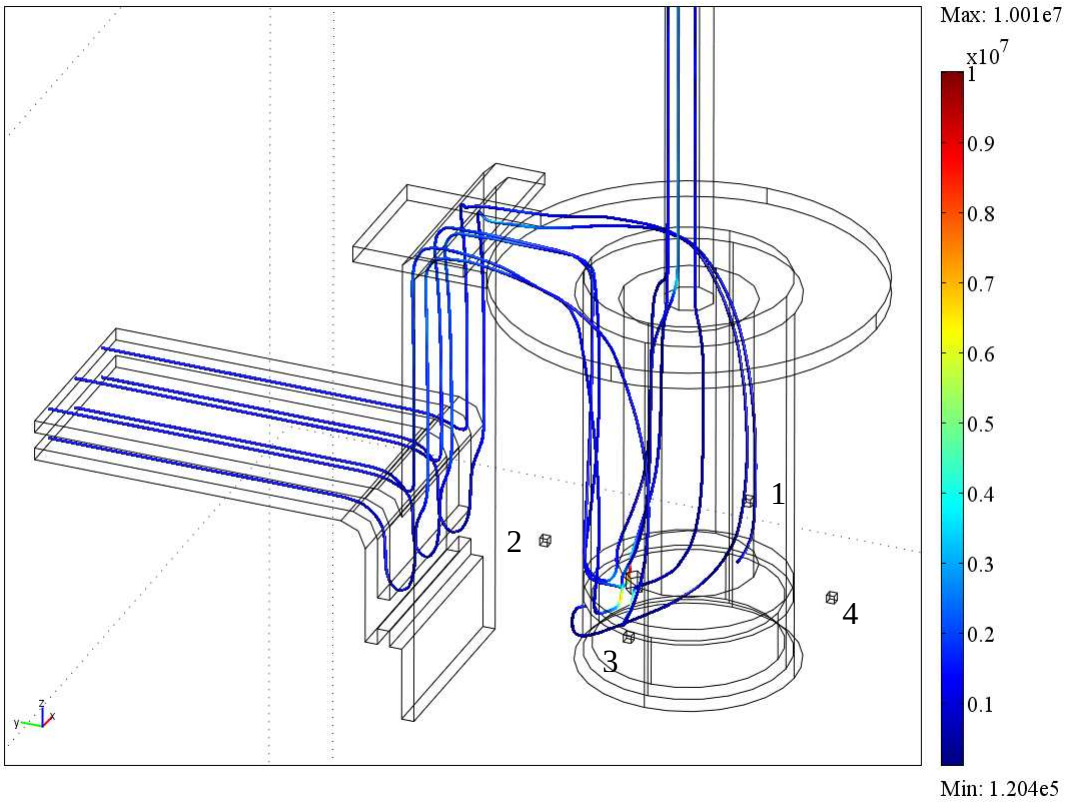

Figure 17 : FEA of current path for 6-inch In 625 melt with offset arc. Streamlines are colored by current density (A/m^2). Input current was 4662 A.

Figure 18, on the following page, shows the resulting magnetic flux density for the simulation.

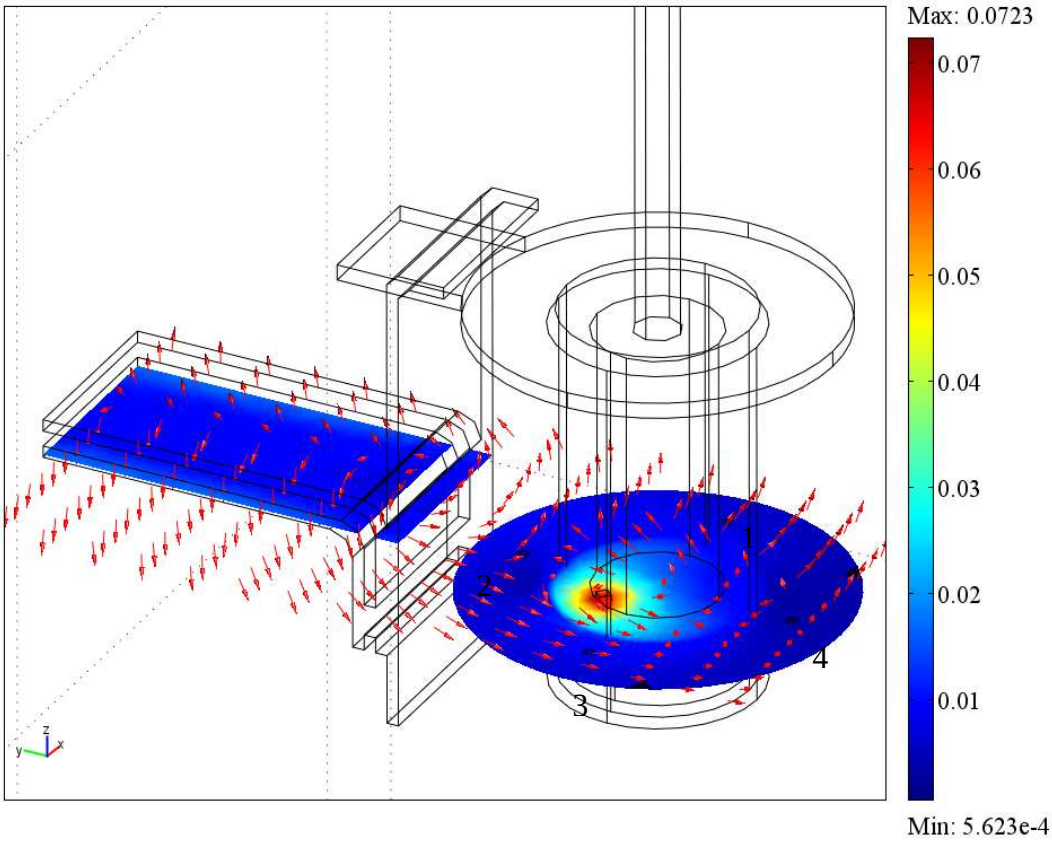

Figure 18 : FEA of magnetic flux density for 6-inch In 625 melt with offset arc. Colored slice indicates the normalized magnetic flux density (T) and arrows show the normalized direction.

It can be seen that a comparatively large magnetic flux density is located around the arc, with a maximum of 723 Gauss. The accuracy of this number will depend on the diameter of the actual arc, in the simulations the arc was modeled as a cylinder with a diameter of 0.5 inches.

The primary purpose in showing the preceding results is to visualize the set-ups for the experiments conducted. Visualizing the models also yields insight into expected magnetic flux density conditions during NETL VAR operation.

Deterministic Equations

The value of the FEA simulated magnetic flux density vector at each of the 4 sensor locations was output for each FEA model. A method was needed to use these VAR simulation results to predict an arc location based on the measurements during the VAR experiments.

A continuous solution was desired so that the predicted arc positions would not be mathematically limited to the arc locations that were simulated. The realization of such a solution also makes excessive simulations unnecessary. An effective solution was found by looking at how the problem might be approached analytically.

For a known current vector, the magneto-static Maxwell-Ampere equation can be solved using what is known as the Biot-Savart Law as stated in equation 6. [20]

$$B(P) = \frac{\mu_o}{4\pi} \int \frac{Ix\hat{\eta}}{\eta^2} dI \qquad (6)$$

B(P) is the magnetic flux density at a point in space (Teslas). The integration is along the current path in the direction of flow, and *dI* is an element of length (m) along the current *I* (Amps), η is the vector from the source to the point. Also, μ_o is the permeability of free space which is equal to the quantity 4π x 10^{-7} N/Amp^2. As previously mentioned, the furnace contains materials that have nearly the same permeability as vacuum, so this quantity can be used.

Even further simplification can be performed in the case that the known current is straight and of infinite length. This simplifies the Biot-Savart equation to equation 7. [20]

$$B(P) = \frac{I\mu_o}{2\pi d} \qquad (7)$$

The term *d* is the distance (m) from the current to the point of interest. This is the simplest way to calculate a magnetic flux density due to electrical current, but in a VAR furnace additional terms are needed.

The electrical currents in the VAR can not be described by a single vector. However, if the parts in the furnace are thought of as conductors in series, then there are three significant current vectors. These are the bus bar vector, the crucible vector, and the arc/electrode vector. These vectors all primarily point in the axial (*z*-direction) and if a collinear assumption is valid, vector super position can be used to solve for the resulting x and y magnetic flux densities at a point using equations 8 and 9.

$$B_x = \frac{z_b \cos(\Theta_b) I_b \mu_o}{2\pi d_b} + \frac{z_c \cos(\Theta_c) I_c \mu_o}{2\pi d_c} + \frac{z_a \cos(\Theta_a) I_a \mu_o}{2\pi d_a} \tag{8}$$

$$B_y = \frac{z_b \sin(\Theta_b) I_b \mu_o}{2\pi d_b} + \frac{z_c \sin(\Theta_c) I_c \mu_o}{2\pi d_c} + \frac{z_a \sin(\Theta_a) I_a \mu_o}{2\pi d_a} \tag{9}$$

In this equation the subscripts *b*, *c*, and *a* stand for the bus bar, the crucible, and the arc vectors respectively. Θ is the angle and *d* is the distance from the sensor to the respective current vector; *z* is the respective view factor from the sensor to the respective vector's end points since the current vectors can not be assumed to be of infinite length. This term is calculated using equation 10.

$$z_i = 0.5(\sin(\Theta h) - \sin(\Theta t)) \tag{10}$$

Where Θh is the angle between a line perpendicular to the sensor and the vector and the head of the vector Θt is the angle between a line perpendicular to the sensor and the vector and the tail of the vector. The location of the tails and heads of the vectors are based on the physical geometry of the system. For example, the tail of the crucible vector corresponds to the z-direction location of the top of the crucible.

If this were truly a coaxial furnace, then the bus bar vector would be zero, and in the case where the arc was exactly centered, the crucible and arc vectors would cancel. The calculated magnetic field would then be zero, as is true for an ideal coaxial VAR.

To solve the problem using these equations, the location of the crucible and the bus bar vector would have to be fixed. This leaves the two unknowns d_a and

Θ_a which are the distance and direction from a sensor to the arc respectively. To ensure the two equations yield a solution for these two unknowns, the equations were re-arranged using MATLAB's Symbolic Math toolkit. Two solutions for the location of a current were found for a given magnetic flux density vector, but one could be eliminated because the polarity of the currents in the system are known.

It was postulated that despite the complicated interdependencies of the current paths, the discrete FEA simulation results could be fit into similar Biot-Savart vector superposition equations that would also allow a continuous prediction of the arc location. Equations 7 and 8 can be simplified into a more generic form with the common terms separated out, and the superposition being thought of as being between a current vector that changes position, and a current vector that does not change position. This idea yields equations 11 and 12.

$$B_x = m_x I\left(\frac{\sin(\Theta_a)}{d_a} - a\right) \tag{11}$$

$$B_y = m_y I\left(\frac{\cos(\Theta_a)}{d_a} - b\right) \tag{12}$$

where B_y and B_x are the FEA simulated magnetic flux density at a sensor's location, Θ_a is the angle from the sensor to the simulated arc position, d_a is the distance from the sensor to the simulated arc position, *I* is the simulated current in Amps. By simulating a number of currents and arc positions a data set is created and then a regression is performed to fit the data to an equation and find the parameter m_x, m_y, *a* and *b*. These parameters are unique to the furnace set-up and to the individual sensor positions.

For each regression, data from at least 7 different discrete arc locations, and three different currents were used. The FEA simulation data fit to the equations quite well. Table 2 shows the result of the regressions for the 4 types of experiments performed.

Table 2 : Resulting regression parameters for the fit of the FEA data to a continuous solution based on the Biot-Savart Law.

FEA analysis:	Static	4” In 625	6” SS 316	6” In 625
1 m_x	0.00195	0.000634	0.000456	0.00153
1 a	-2.87	-7.3	-9.1	-3.99
1 r^2	1.00	1.00	1.00	1.00
1 m_y	-0.00176	-0.000318	-0.000261	-0.00073
1 b	-7.25	-5.1	-5.1	-7.14
1 r^2	1.00	1.00	0.99	1.00
2 m_x	0.00176	0.000333	0.000243	0.000738
2 a	-17.90	-34.2	-39.1	-20.47
2 r^2	1.00	1.00	1.00	1.00
2 m_y	-0.00198	-0.000639	-0.000472	-0.00150
2 b	-2.74	-4.7	-4.6	-2.48
2 r^2	1.00	1.00	1.00	0.99
3 m_x	0.00198	0.000636	0.000499	0.00149
3 a	-2.18	-5.7	-6.6	-3.14
3 r^2	1.00	1.00	1.00	0.99
3 m_y	0.00175	-0.000323	-0.000270	-0.000749
3 b	6.50	1.8	1.50	5.83
3 r^2	1.00	1.00	0.99	1.00
4 m_x	0.00174	0.000317	0.000257	0.000742
4 a	5.53	-2.7	-4.7	4.16
4 r^2	1.00	1.00	1.00	1.00
4 m_y	-0.00196	-0.000629	-0.000467	-0.00149
4 b	-0.21	-0.59	-0.80	-0.31
4 r^2	1.00	1.00	1.00	0.99

As it can be seen in this table, the fit parameters are unique to each type of melt and to each sensor. This is due both to the location of the sensor along the furnace axis, the height of the ingot, and the crucible used. The 6-inch melts used the same crucible as the static tests.

A comparison of equation parameters between runs, as well as between individual sensors can be made. Considering the goal is to measure a change in current

density location, the best signal to noise (S/N) ratio will have the largest m_y and m_x and the smallest *a* and *b* parameters. Not surprisingly, the highest S/N is for the static test simulation, where the entire length (13”) of the electrode is moved about. This is versus the melt test simulations, where only a 0.5” in length arc is moved around. Due to the bus bar, the *a* term is largest for sensor 2. This implies sensor 2 has the lowest S/N ratio among sensors.

To verify that the equations work, the simulated magnetic flux densities for different FEA simulations are used as inputs to the equation. Verification of the predicted arc location to simulated arc location can then be performed. Figure 19 shows the 7 different simulated arc positions, and the resulting prediction using the equations for the 4-inch In-625 melt. The input current was 3000A.

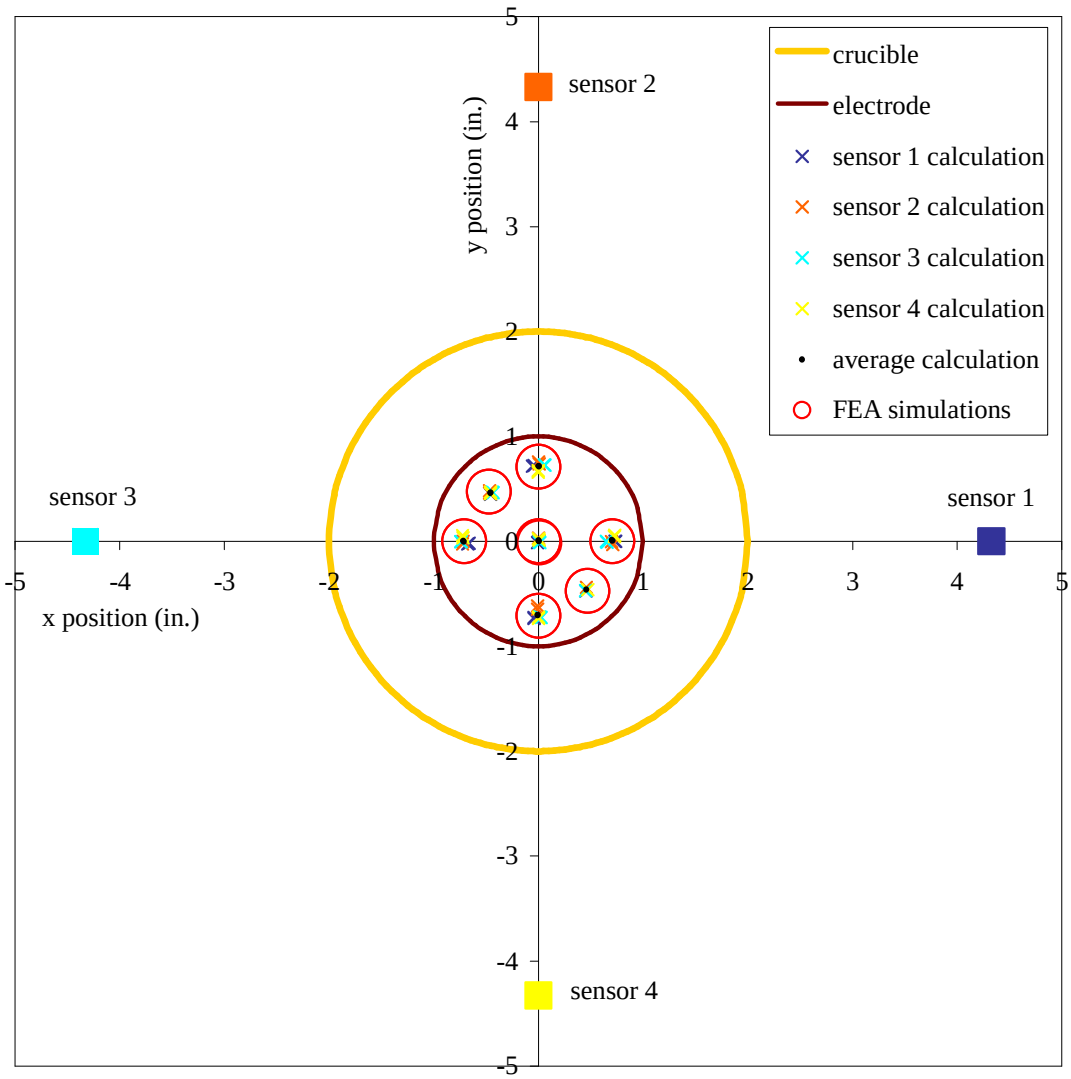

Figure 19 : Verifying the equation for 4 inch In 625 FEA simulations

This shows that fitting magneto-static FEA data to analytical equations based on the Biot-Savart law works quite well. Essentially COMSOL can be thought of as the calibration tool which provides a continuous, deterministic, and sensor independent arc position solution.

Static Test Validation

As a control to test the electric arc location system, tests were performed in which no arcing took place. The tests are referred to as static because the electrical path does not change during the test, as would happen in the presence of a dynamic electrical arc. In actuality, these control tests are not static because the electrical current is varied, albeit very slowly, versus time. The experiments were performed in the coaxial VAR chamber, using the same 6-inch crucible that would later be used in some of the melt experiments. Tests were run for five discrete electrode x-y positions, and one additional test to look at set-up repeatability. This involved a graphite electrode and a machined plate to accommodate 5 discrete positions of the electrode relative to the crucible.

The procedure for this test involved turning on the current, and holding it at three distinct values such as 1000Amps, 2500Amps, and 4000Amps. The resultant magnetic flux densities were recorded at each sensor position.

Data for the static experiments were sampled at 3000Hz, and then averaged to 30Hz prior to logging to file. The time averaged electrode location results over the duration of each experiment can be seen plotted together in an overhead view in Figure 20.

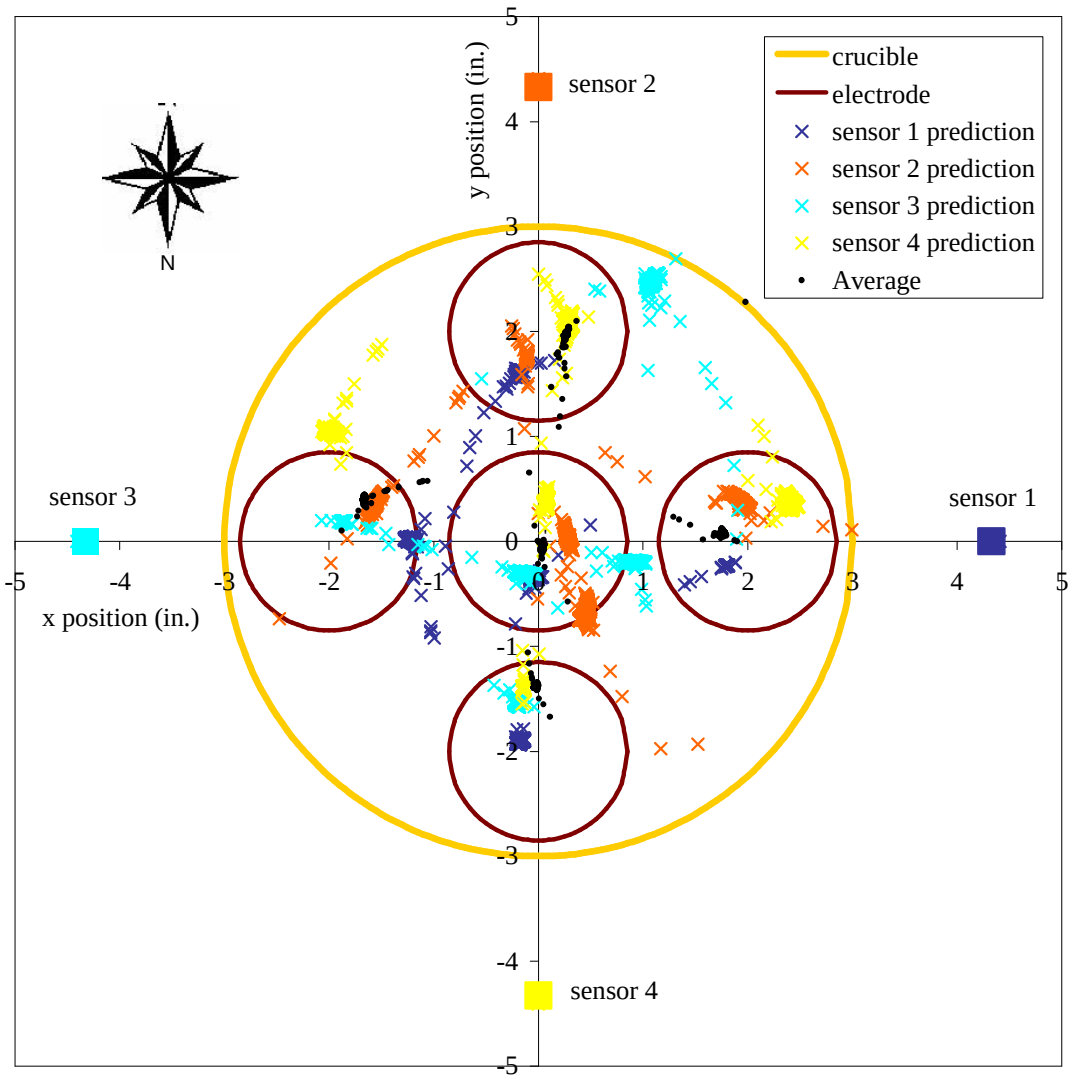

Figure 20 : Calculated electrode position from each sensor for the five static tests on the same plot.

The overhead orientation is the same as seen in Figure 7; sensor 2 is closest to the bus bar. For the static test with the electrode in the center, the predicted location for all four sensors agrees with the location of the center of the electrode to within about 0.5 inches. Averaging the predictions of the four sensors correctly locates the center of the electrode. If the positions of the electrode in the furnace, as indicated in the figure, are correct then the predictions that show the most error are sensor 2 for the

north position test, sensor 4 for the east position test, and sensor 3 for the west and south position tests. Overall, the predicted electrode displacements for physical electrode displacement are in the correct direction for each sensor, indicating the analysis method is working. For example, when the electrode is moved in the north direction, the predictions also move in the north direction, and when the electrode is moved in the east direction, the predictions move in the east direction.

There does appear to be a trend of the predictions toward the center of the furnace. It is thought that this is due to a systematic error in the set-up of the parts inside the furnace.

A repeatability test of the center static test yielded individual sensor electrode predictions that all moved toward sensor 4 by about 0.25 inches. This involved removing and then replacing the electrode assembly. This demonstrates that there is some non-systematic uncertainty in the predictions due to the set-up. However, since the sensor's predictions all moved together, the discrepancy in predictions between sensors are likely caused by a different source of uncertainty. For example, the value of the shunt resistor used to measure the system's current could be incorrect. Also, the crucible is not fixed to the furnace, so it may not have been exactly centered in the furnace. Efforts were not taken to ensure accurate physical location of the furnace parts, as the primary purpose of this study was to investigate the general behavior of external magnetic fields for future study.

In the above static result figures, a few data points can be seen that are off from the others and seem to follow a trail away from the bulk of the predicted points. These are due to the single point surges in the current data that can be seen in the time domain data section of the results chapter. Essentially, they are an error. Also, the locations of calculated positions are slightly skewed in this same direction. Further investigation of this reveals that this occurs during current ramp up, as opposed to a shift versus time or overall current. So position calculation is independent of current at steady state, with some effect at current ramp ups, and larger errors at extremely fast current transients.

Overall, the static tests validate the developed magnetostatic equations to calculate the position of a current source inside the furnace. Data for the static tests also give a reference for what magnetic field data look like without the presence of arcs.

Overall key assumptions for the analysis are:

1. that the bandwidth limitation of the instrumentation is sufficient to characterize arc behavior
2. that the magnetostatic equations are applicable
3. that there is a single arc at any given instant during the test
4. that all of the current, as measured by the shunt, channels through the arc at any given instant
5. that the arc is parallel to the axis of the furnace and has a cylindrical shape
6. that the axial location of the electrode gap can be neglected for the experiments performed
7. that there is not any time varying current behavior due to the current path in the electrode or through the boundary between the ingot and the crucible

These assumptions are by no means believed to hold true. However, making them provides a simplification that allows for the deterministic arc location results. Most of these assumptions are examined along with the results.

Results and Discussion

Data from four melts using the NETL experimental coaxial VAR furnace are presented. Analysis was performed using a developed LabVIEW Virtual Instrument (VI), with embedded MATLAB math script to perform the arc location calculations. The front panel that controls this VI can be seen in Figure 21.

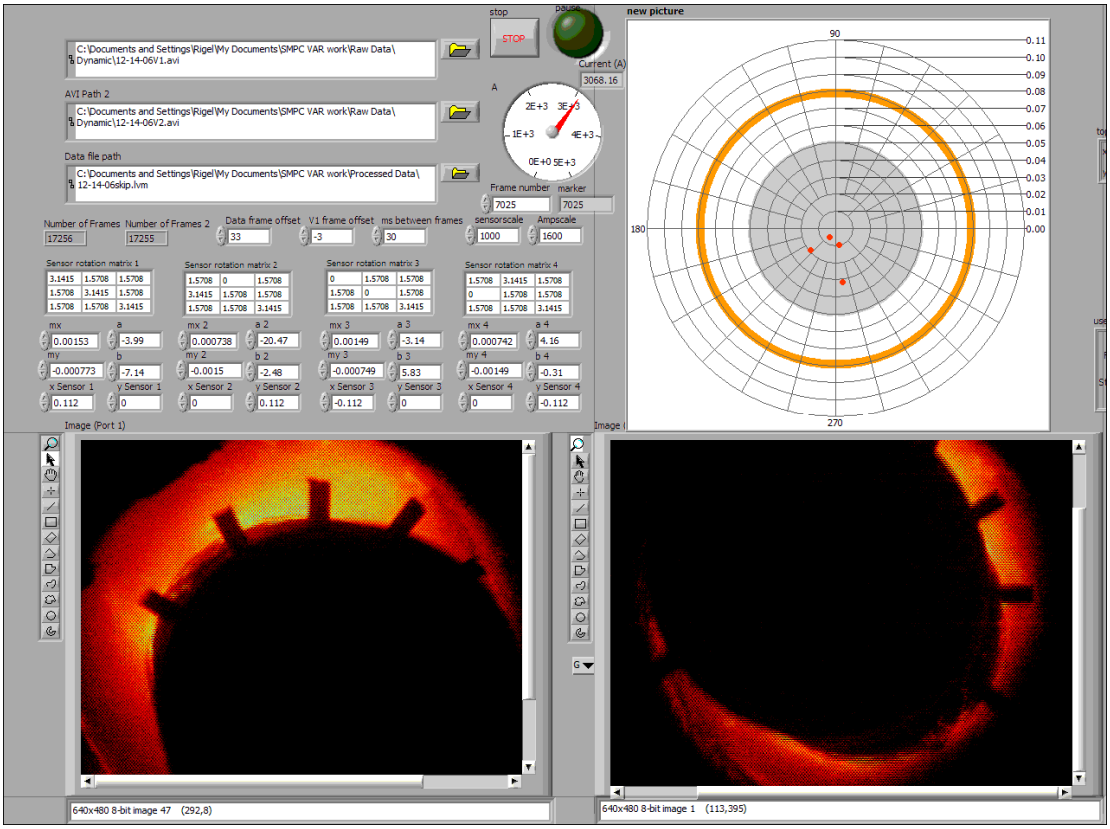

Figure 21 : The arc location analysis VI front panel

The inputs to the arc analysis VI are the data file path, the video file paths, the location of each sensor, the sensor rotation matrices to transform the acquired data from a cylindrical coordinate scheme to the Cartesian coordinate scheme, the sensor

and current scale factor dictated by the instrumentation, a frame offset input for the video versus the data, and the FEA simulation analysis parameters for each sensor. Also, the VI can run at a user input rate, or individual data points can be accessed. The output is a digital current indicator, two bore site videos with a gradient processing filter applied to bring out changes in intensity, and an overhead map showing the predicted arc location according to each sensor. The analysis results can be output to a file. Other VIs were created to input simulated data signals with varying frequency content, or noise simulations into the analysis algorithm. Also, a VI was created to test the analysis with manually input magnetic flux density and current data.

First, some of the acquired signals will be presented in the time domain. This gives an overview of the signals measured during a test. The signals during a melt are compared to the signals taken during a static test. Second, time averaged arc location results are presented. This type of analysis is useful to identify the presence of non-axisymmetric, constricted arc distributions. Also, this analysis shows whether there is any change in this distribution over the course of VAR operation. Third, instantaneous arc location results are examined. The validity of the single arc assumption and the magnetostatic assumption is questioned. Finite element analyses of scenarios with multiple arcs are presented. Finally, an in depth analysis of the frequency and directions of motions seen in the results are analyzed. The frequency domain is analyzed using FFT. Signal simulation and noise analysis is utilized to help explain the results. Event motion of the calculated movement of the arc is correlated to video data acquired at the same instant.

Time domain Data

The time domain data for the static center experiment is shown in Figure 22. A nested picture gives an overhead view of the location of the sensors, the crucible, and the electrode. Recall from Figure 7 that each sensor actually contains three independently measured orthogonal sensing elements called *x*, *y* and *z* which are not orientated in a Cartesian coordinate system.

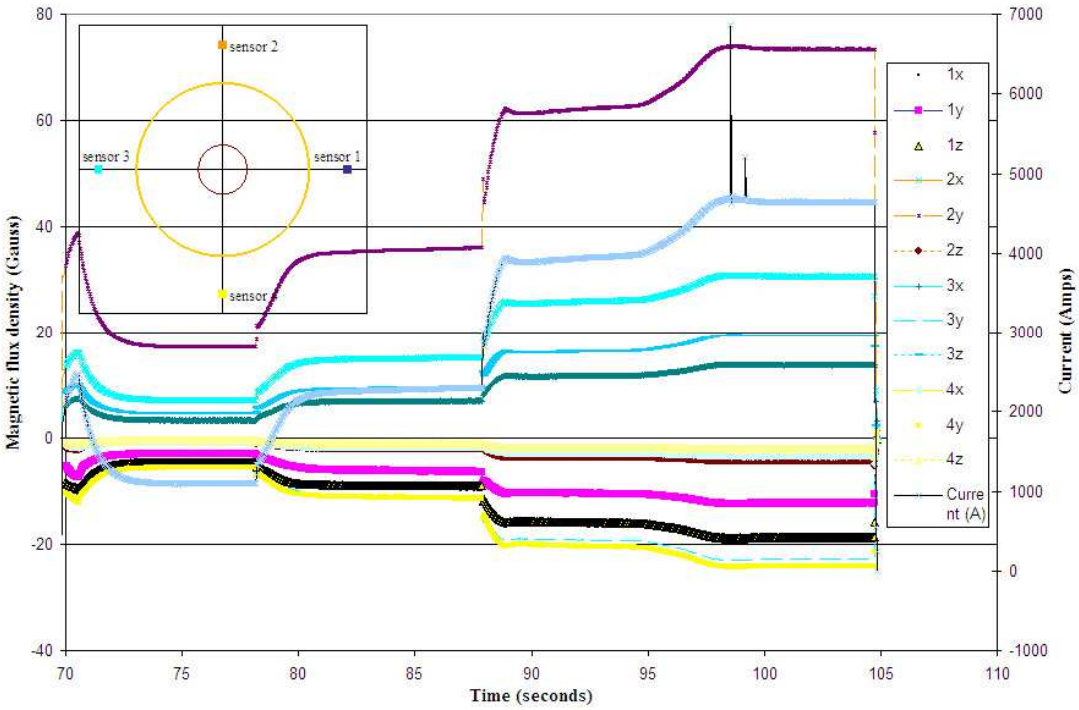

Figure 22 : *B* and *I* versus time for static center test #1. Data are averaged from 3000Hz sampling rate to 30Hz.

The sensing element measuring the largest magnetic flux response is 2y, which makes sense because this sensor is closest to the bus bar. The y-axis primarily measures current moving in the axial direction. A true coaxial furnace would show zero magnetic flux density for all elements for the centered case, regardless of the current. So the bus bar side of the furnace shows the most deviation from how a coaxial furnace should respond.

As soon as the current increases, the magnetic flux density follows. The increasing current seen is due to the operator increasing the current. The exception is there are a few single data point spikes in the current data that are not reflected in the magnetic data. These spikes are then either errors in the current measurement, or actual surges in current that are faster than the response time of the magnetic sensors.

A measurement error of that magnitude is unlikely, so it is reasonable to assume that it is some kind of surge. Also, since there isn't any melting or arcing taking place in these experiments, it is reasonable to assume these spikes are related to the power supply, and not due to something occurring inside the furnace. Transients from the AC power grid getting through are a likely culprit.

Finally, the time domain data shows that the *z* element does not respond to movement of the electrode or a change in current very much. This element is primarily responding to current moving in the radial direction so this makes sense. The *z*-direction is not needed in the arc position analysis.

Figure 23 shows the time domain data for a melt that used the same crucible as the static experiment.

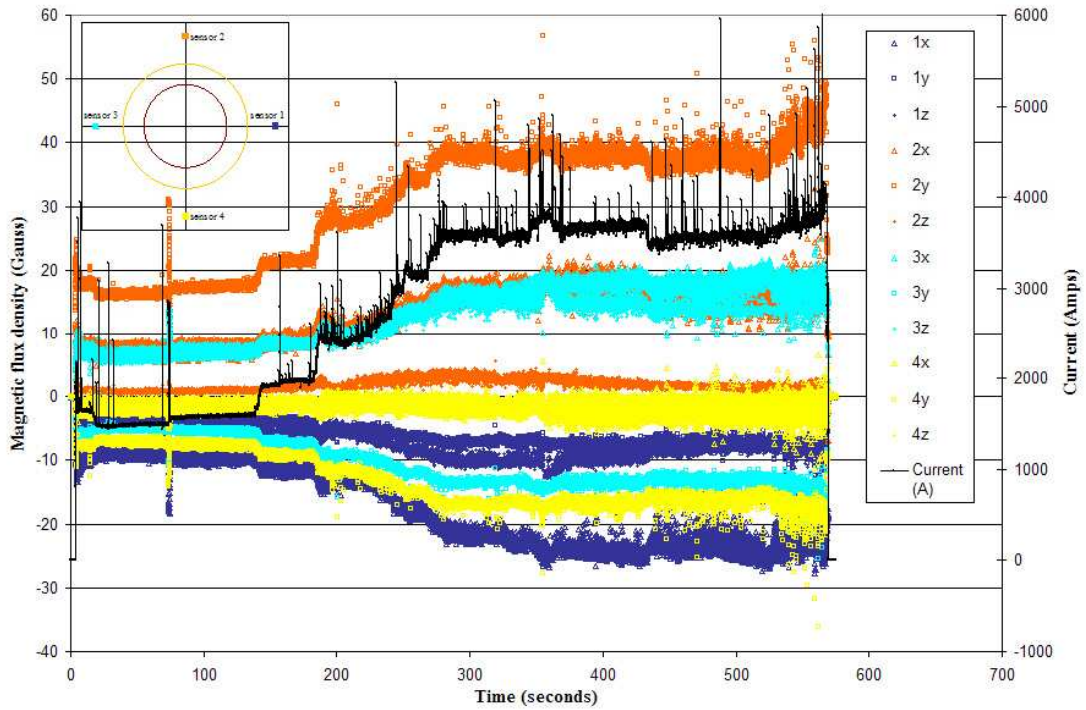

Figure 23 : *B* and *I* versus time for 6-inch In 625 melt. Data are averaged from 3000Hz sampling rate to 30Hz.

Similar to the static tests, the largest magnetic flux response is coming from 2y, due to the bus bar. Also similar, the magnetic flux data increases and decreases with the current. Differing from the static tests, it can be seen that the magnetic flux density varies quite a bit. The current also shows more variation. Current variation is expected during VAR operation because of the varying resistance to the flow of current across the gap between the ingot and electrode. However, the current variations alone cannot explain the variation seen in the magnetic flux density data. This additional content could be the signal of interest, which is a flux due to a moving arc. Still, the change in the magnetic flux due to any arc movement is fairly small compared to the response of the magnetic field versus the current.

As mentioned, the z-direction is not used in the analysis. However, it is worth looking at because variations in this channel could also mean variations in the x and y channels. For example, if the current path through the ingot shelf varies with arc position then the effect would be most pronounced in the z-directions sensing element. Figure 24 shows the z-direction data in the time domain for one of the experiments.

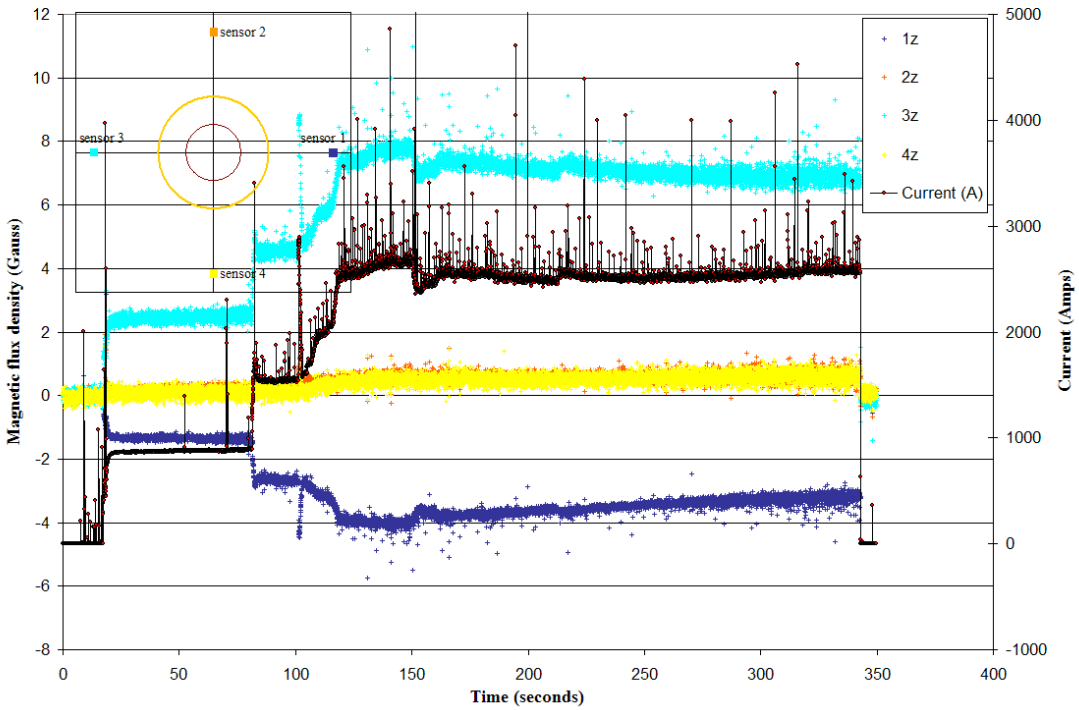

Figure 24 : *Z*-direction *B* and *I* versus time for 4-inch In 625 melt data.

This figure shows a clear slight trend of the z-direction magnetic flux density versus time. The current remains fairly constant, but the magnetic flux is changing. This constant slope supports the idea that this change is due to z-direction movement of the electrode gap. No periodic changes are seen in the z-direction data, as would be observed if there was significant changing of the ingot to crucible boundary condition. Therefore, the assumption that this effect can be neglected seems valid.

Time Averaged Arc Locations

Time averaged arc location data are important because this can provide information that would allow for calculation of quasi steady energy input into the ingot pool. As previously discussed, this will have implications to the formation of defects.

First, it is worth mentioning what a diffuse arc distribution would look like since this is the benchmark for quality VAR operation. A diffuse arc condition would result in a distinct collection of predictions smaller than the diameter of the ingot, and with all 4 sensors agreeing on the predictions. The area of coverage of the distribution over the duration of the melt would then be directly related to the number of data points averaged, with an increasing number of averages resulting in a decreasing predicted distribution area.

The data was acquired at 3000Hz, and then averaged to 30Hz so each point represents the average of 100 data points. Figure 25 **s**hows the time averaged results for the duration of the first melt experiment. This consisted of melting a 2-inch diameter solid bar of Inconnel (In) 625 into a 4-inch diameter copper crucible. In 625 is a type of nickel alloy.

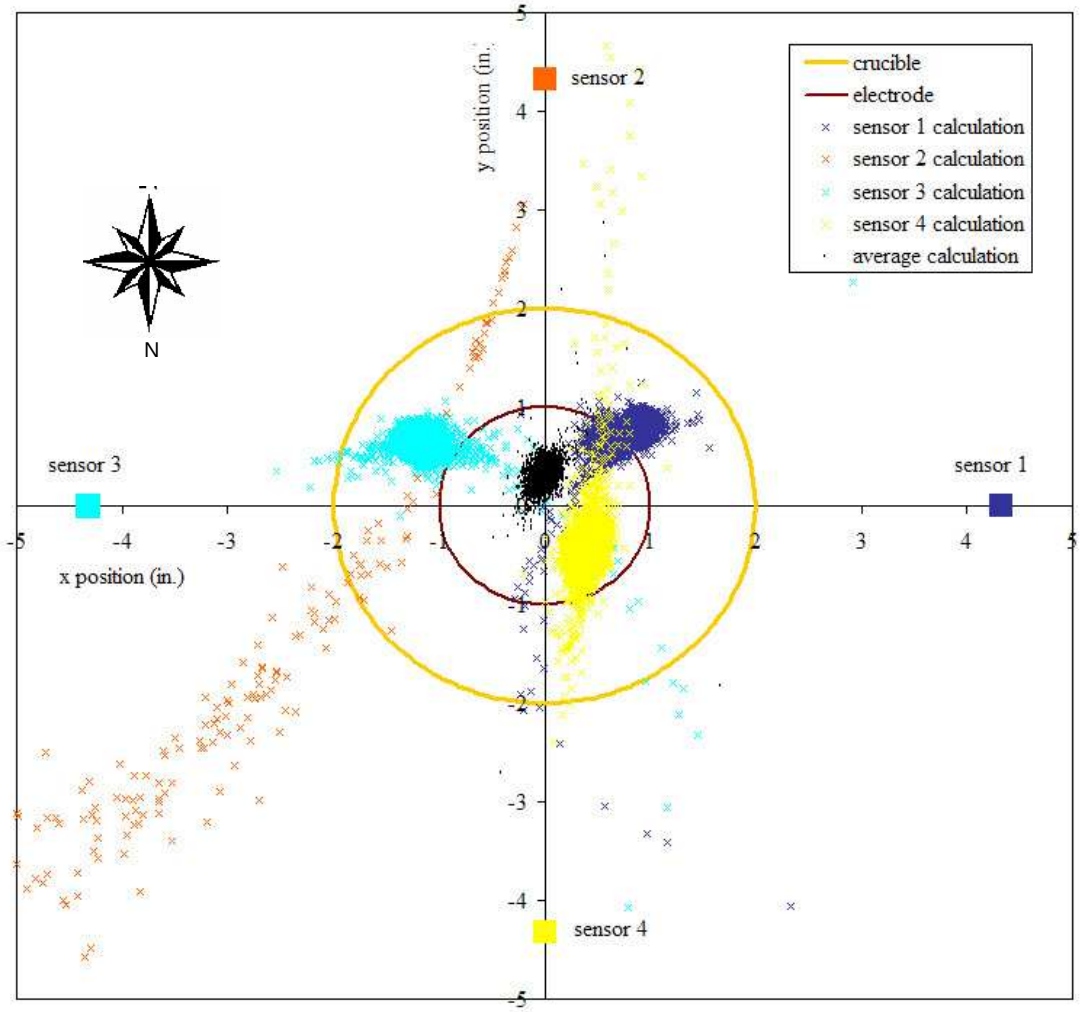

Figure 25 : Time averaged arc locations for 4-inch In 625 test #1.

Sensor number 2 places the predicted location of the arc off the map, which of course is not possible. The bus bar is the likely source of error causing this, because sensor 2 is closest to the bus bar. The other sensors are likely also affected by this error, which might explain some of the disagreement. The plotted average does not include data from sensor 2. The average predicted arc location is on the south side of the electrode, toward the bus bar. It should be mentioned that the plot shows a dot representing the center of the arc, and does not reflect the width of the arc. Since this test used the 4-inch crucible, it is difficult to compare the accuracy of the location

predictions to that seen in the static tests which used the 6-inch crucible. Figure 26 shows the results for another 4-inch In 625 melt.

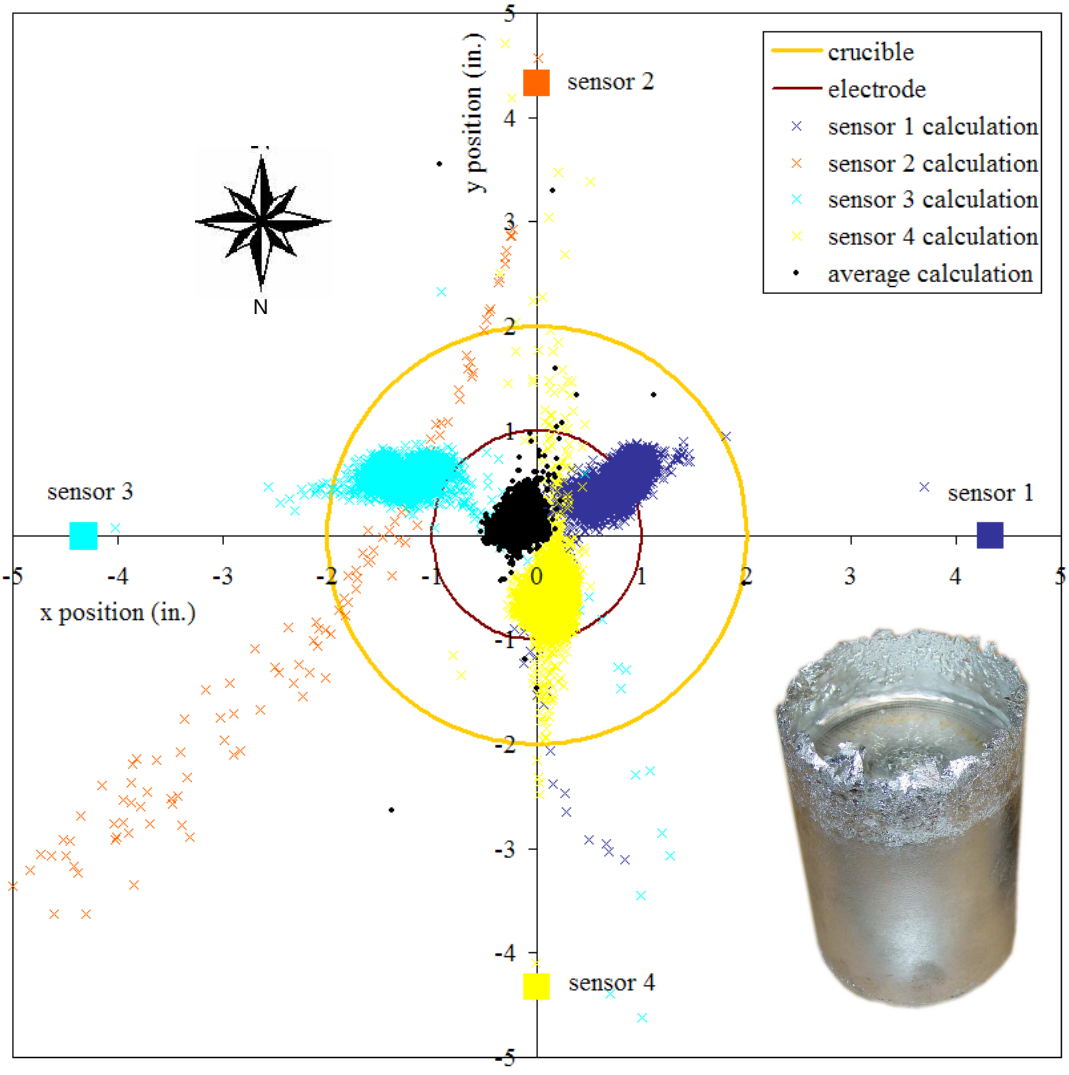

Figure 26 : Time averaged arc locations for 4-inch In 625 test #2.

This shows consistency in the results for identical melt conditions. It can be seen that the analysis is not overly sensitive to the small amount of differences between experiments. Also, shown is a picture of the formed ingot after removal from the VAR.

The results show an off centered distribution that would be consistent with constricted arc conditions. The disagreement between sensors shows the accuracy in location could be off, but it is worth looking at the remainder of the electrode to see if there is any corroborating evidence for a constricted arc in this direction. Figure 27 shows the remains of the electrode for the 4-inch In 625 melt. The interesting thing is that there does appear to be more material melted off in the south direction, toward the bus bar. This is consistent with the time averaged arc location data presented.

Figure 27: The leftover electrode after the 4-inch In 625 melt #2. Note more material melted off in the direction of the bus bar (and sensor 2).

In addition to favoring the bus bar side, there exists an overall convex electrode tip shape that suggests the arc is more often toward the edges, and less often in the middle. This is also the general observation for melts performed in this furnace. Diffuse arc conditions will result in a nearly flat electrode surface, so it is likely that constricted arc conditions regularly exist. For a comparison, Figure 3 shows an

electrode tip resulting from diffuse arc conditions in a different furnace. A constricted arc is not surprising given the proximity of the bus bar, which can also be seen in the photo. The bus bar creates a magnetic field that off balances the furnace by creating stronger Lorentz forces in certain directions in the arc region.

Using the 6-inch crucible, a solid bar of 3 inch diameter Stainless Steel was melted. Figure 28 shows the results for this experiment. The final melt was only about 3-inches tall, so the sensors were located fairly close to the bottom of the crucible.

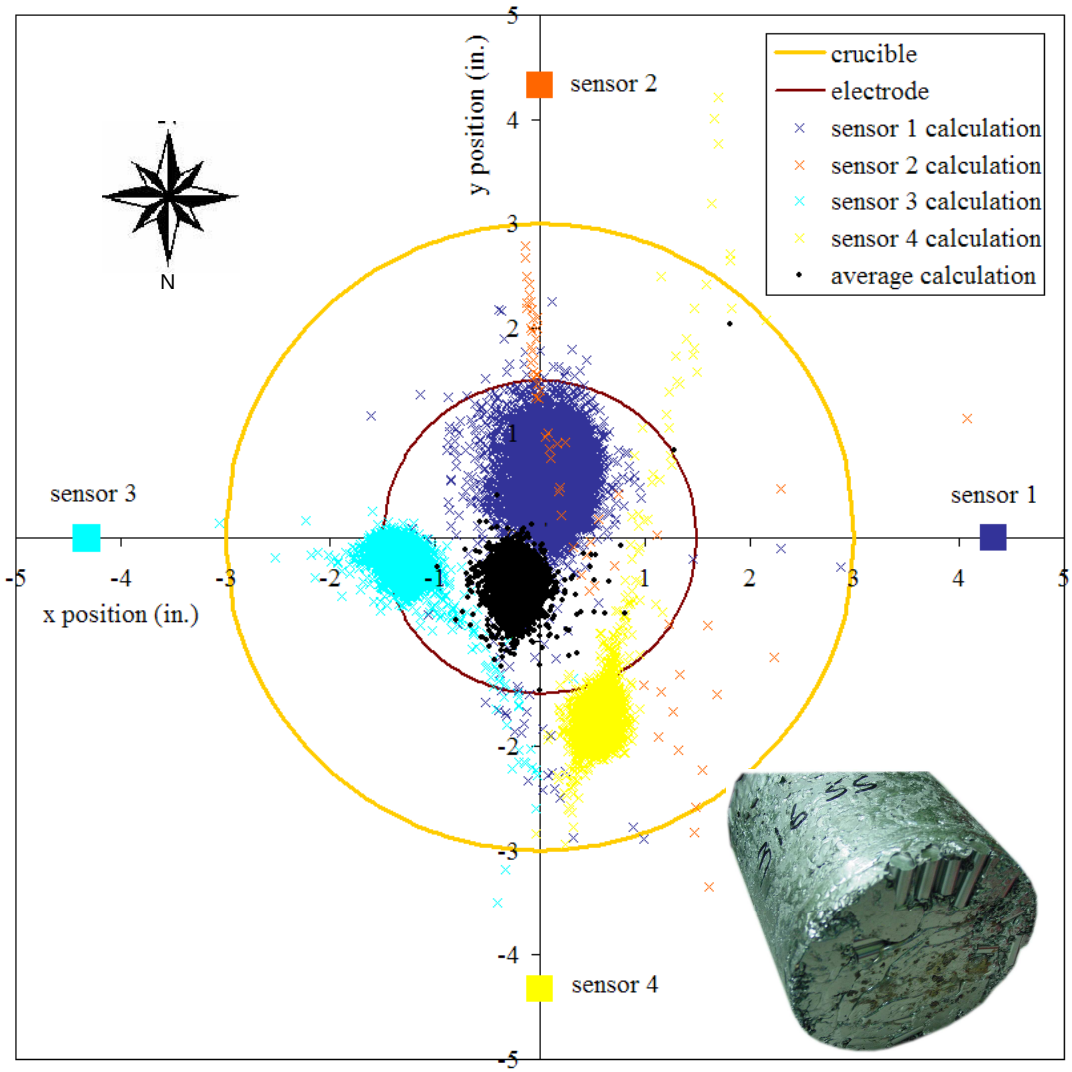

Figure 28 : Time averaged arc locations for 6-inch SS 316 test.

Again it can be seen that sensor 2 fails to predict an arc location inside the chamber, but this time puts the prediction outside a different part of the furnace. Also, sensor 1 shows a much wider distribution than sensors 3 or 4. It is unclear why this is the case. The unmelted pieces showing in the bottom of the ingot indicate that the melt did not use enough power. Unfortunately, a post melt photograph of the electrode tip is not available.

Figure 29 shows the results for the 6-inch In 625 melt. This electrode was formed by welding three 4 inch melts together.

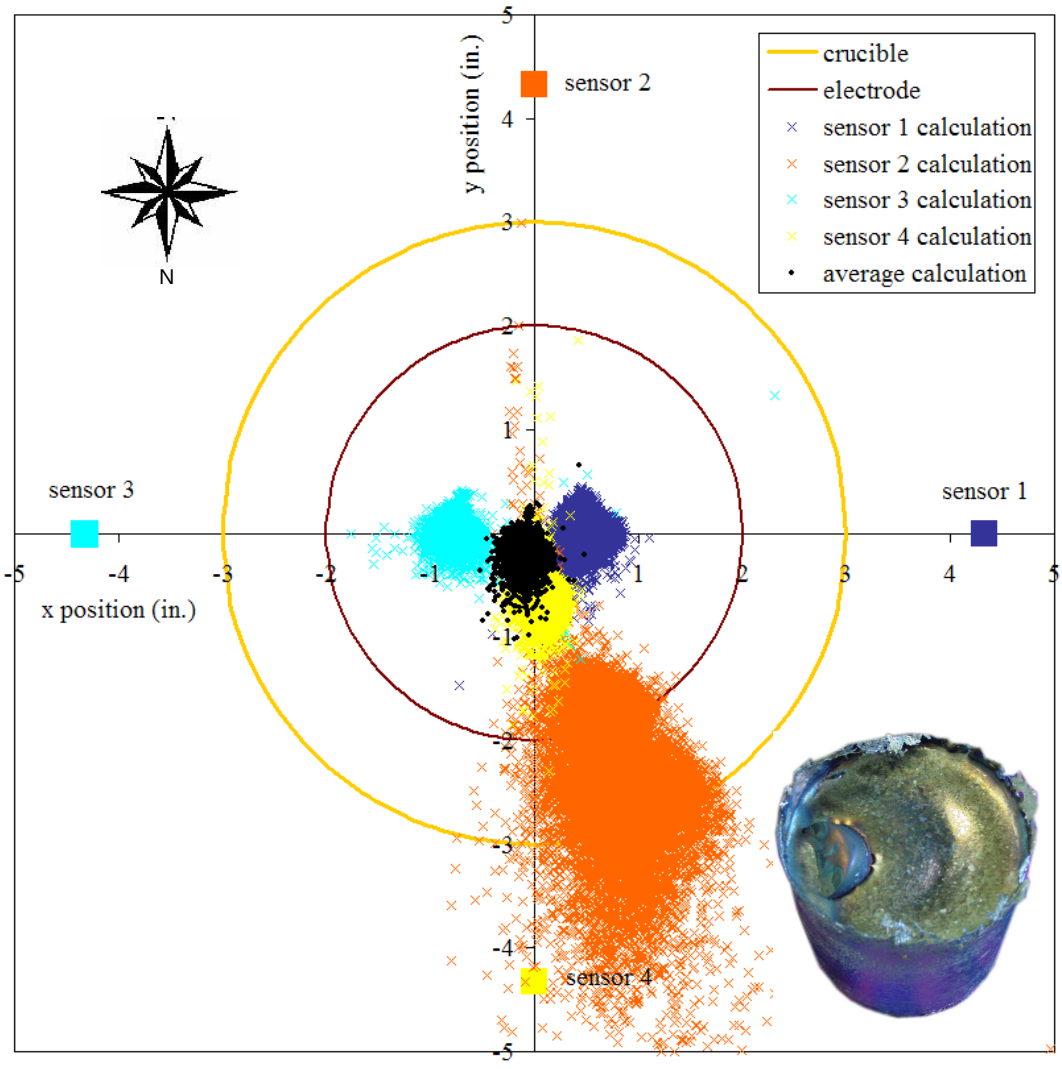

Figure 29 : Time averaged arc locations for 6-inch In 625 test.

Once again sensor number 2 shows a large error, but this time the distribution can be seen on the map. Interestingly, the distribution area predicted by sensor 2 is reduced if the parameters of the solution are adjusted so that the result falls within the expected area of the electrode. This means the predicted arc motion results are not independent from the absolute location results. Therefore, future experimental work should employ more careful positioning of the parts of the furnace with respect to the sensors.

Sensor number 2's error seems to be related to the z-direction position of the sensor, as locating the sensors further up the height of the crucible causes less error. It is therefore likely that the error is not only coming from the bus bar, but it is specifically coming from the 90 degree junction of the bus bar that is located in a plane lined up to near the bottom of the crucible. This is shown as a solid connection in the FEA model, but in actuality it is several plates bolted together. Refinements to the bus bar geometry in the FEA analysis could probably be made to reduce this error.

The anomaly seen in the top of the 6-inch In 625 melt is actually part of the electrode that accidentally fell off into the melt pool at the end of the test. Leading up to this event were some interesting arc conditions which will later be detailed.

Overall, wider distributions are seen for the melt tests compared to the static tests. This is consistent with behavior expected for a moving arc. The distributions cover most of this area in a short time span compared to the length of the experiment. This shows that the arc is not moving around over the duration of the tests as would be the case for slow time scale ensemble arc motion. The lack of movement in the predictions versus current shows the analysis is correctly accounting for changes in DC current. It also validates the assumption that the axial location change of the electrode gap during the course of the experiment can be neglected.

Averaging the predicted arc locations from several sensors appears to be the best method to determine quasi static arc distribution. To further investigate arc distributions, instantaneous data is examined.

Instantaneous Arc Locations

For an experiment, with no signal averaging, it would be expected that the arc distribution would cover most of the electrode surface over the duration of the test, provided the single arc assumption is correct. Of course, the assumption that the bandwidth of the instrumentation is sufficient would also have to be true. Figure 30 shows the predicted arc locations for the 6-inch In 625 melt, when the data is re-sampled from 3000Hz to 30Hz.

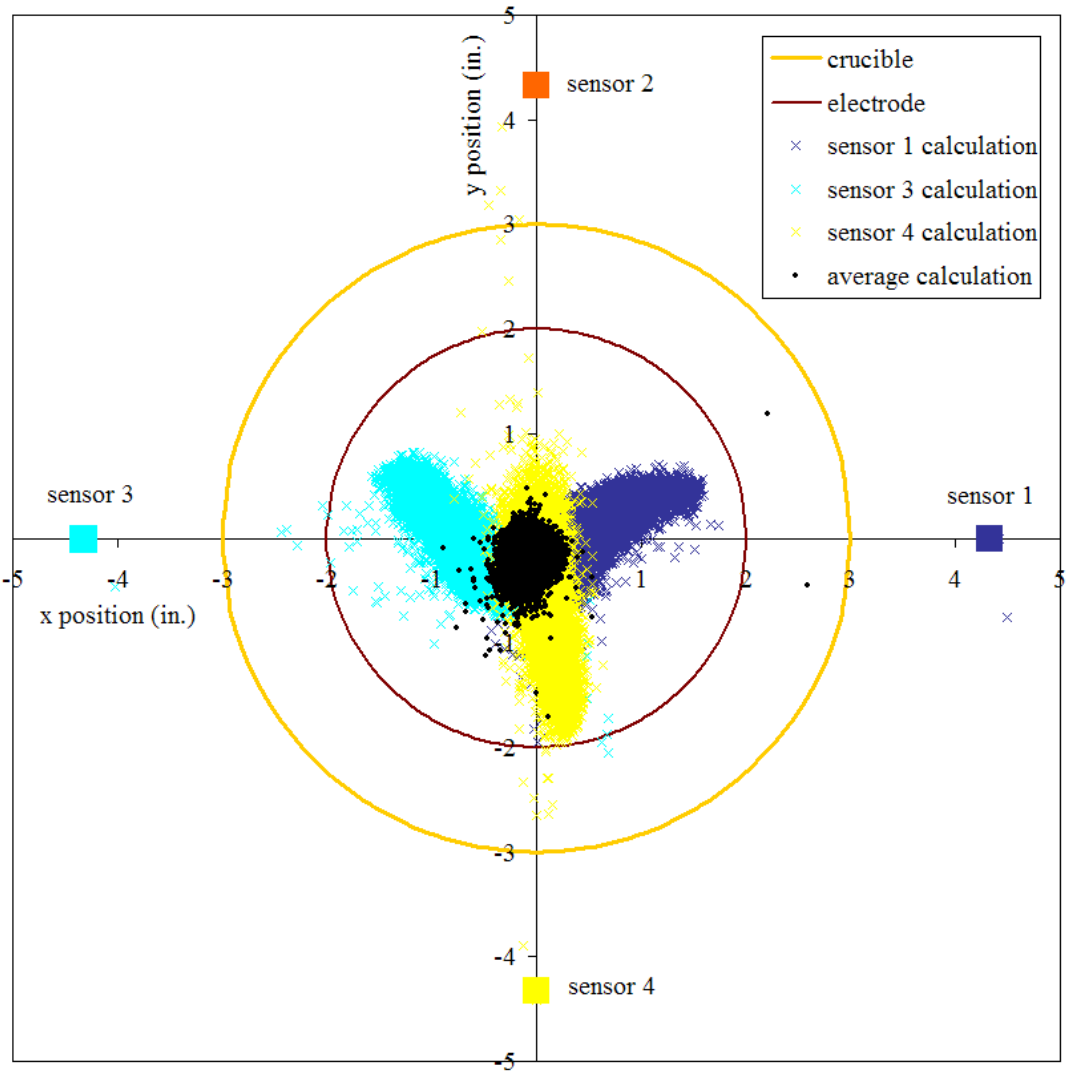

Figure 30: Instantaneous arc locations for 6-inch In 625 melt sampled at 30Hz.

Sensor 2 data was omitted from this figure because this data has a high degree of error, as seen in the last section. The interesting aspect is that the spread of data points appear to diverge from the center to the outside of the electrode, and generally toward their respective sensor. Also of interest is that the average location is more limited in distribution, indicating the motion for the individual sensors is opposing, or in retrograde motion. This causes the displacements to cancel out when averaged. This behavior was observed for all 4 of the melt experiments.

This retrograde motion displays a distinct periodic nature, as will be shown and analyzed in the next section. First, it is worth investigating whether this distribution could be explained by arc motion. A single arc could not cause this effect, so FEA simulations were performed looking at multiple arc scenarios. The resulting magnetic flux density values predicted for these scenarios at each sensor position was then input into the single arc analysis VI to see the effect. Figure 31 shows the result of 4 distinct arcs which are axisymmetric about the axis from the perspective of the sensors.

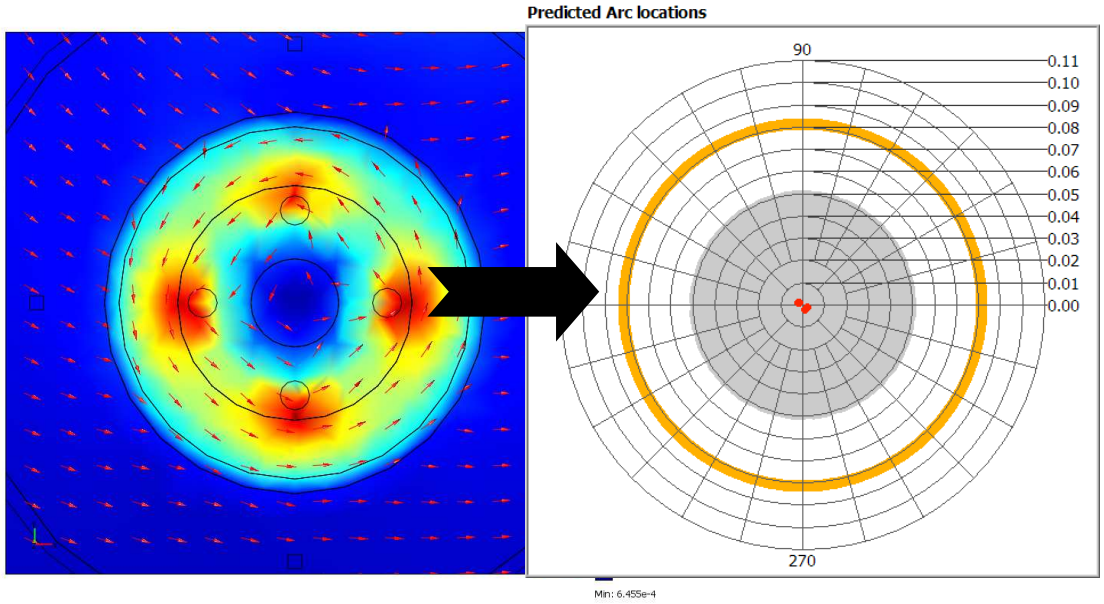

Figure 31 : The effect of multiple nearly axisymmetric arcs on the single arc prediction equations. The result is the same as that for a single, centered arc.

This analysis indicates that the presence of multiple arcs that are axisymmetric will have nearly the same effect on the analysis as a single centered arc would. It is conceivable that axisymmetric retrograde multiple arc motion is limiting the distribution area seen in the instantaneous results. Previous studies have shown radial motion of the arc; this makes sense because this is the same direction that the furnace generated Lorentz force is acting. Further, if multiple arcs are moving axisymmetrically in this way, simple magnetic field vector sensing on the outside of the furnace would have almost no response that would be different than a stationary arc. In other words, this is not a limitation in the analysis but rather in the measurement system itself.

Although axisymmetric multiple arc motions might explain the limited distributions seen, they do not explain the retrograde motion observed. This motion could be explained by multiple arcs that were not axisymmetric. Figure 32 shows the FEA simulation for two discrete arcs and the effect this has on the predicted arc locations.

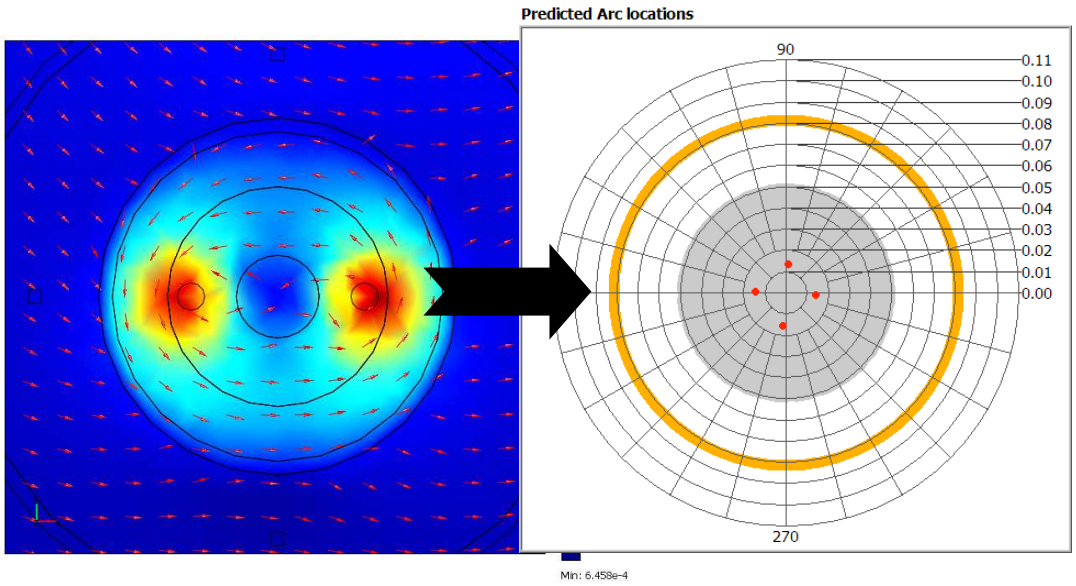

Figure 32 : The effect of a non-axisymmetric multiple arc scenario on the single arc prediction equations. All four sensor predictions diverge from the middle.

This analysis shows the result of simulating two arcs, which causes all 4 sensors' predictions to diverge from the center in retrograde motion compared to arcs grouped in the center. It is also important to note that the movement is attenuated, the arcs in the simulation are all the way toward the edge, but the sensor predictions only move about half that distance. Still, this shows that retrograde motion is possible to see in the analysis as the result of multiple arcs that are oscillating in a manner that is not axisymmetric. If this behavior were real it may be limited specifically to the furnace used in these experiments, because of the unusual presence of the bus bar on one side of the furnace.

The multiple arc scenarios should be considered as the cause for the limited distribution and retrograde motion observed, but this is by no means conclusive. In the next section, the frequency content of the signals is analyzed to further investigate the motion. From this it will be shown that the electric current appears to play a large role in both the frequency and direction of travel for the instantaneous arc predictions.

Periodic Retrograde Arc Motions

To examine the retrograde motions, the full 3000Hz sampling rate data are examined. Figure 33 shows the arc location results for the 6-inch In 625 melt over a half second time frame, or about 1500 data points.

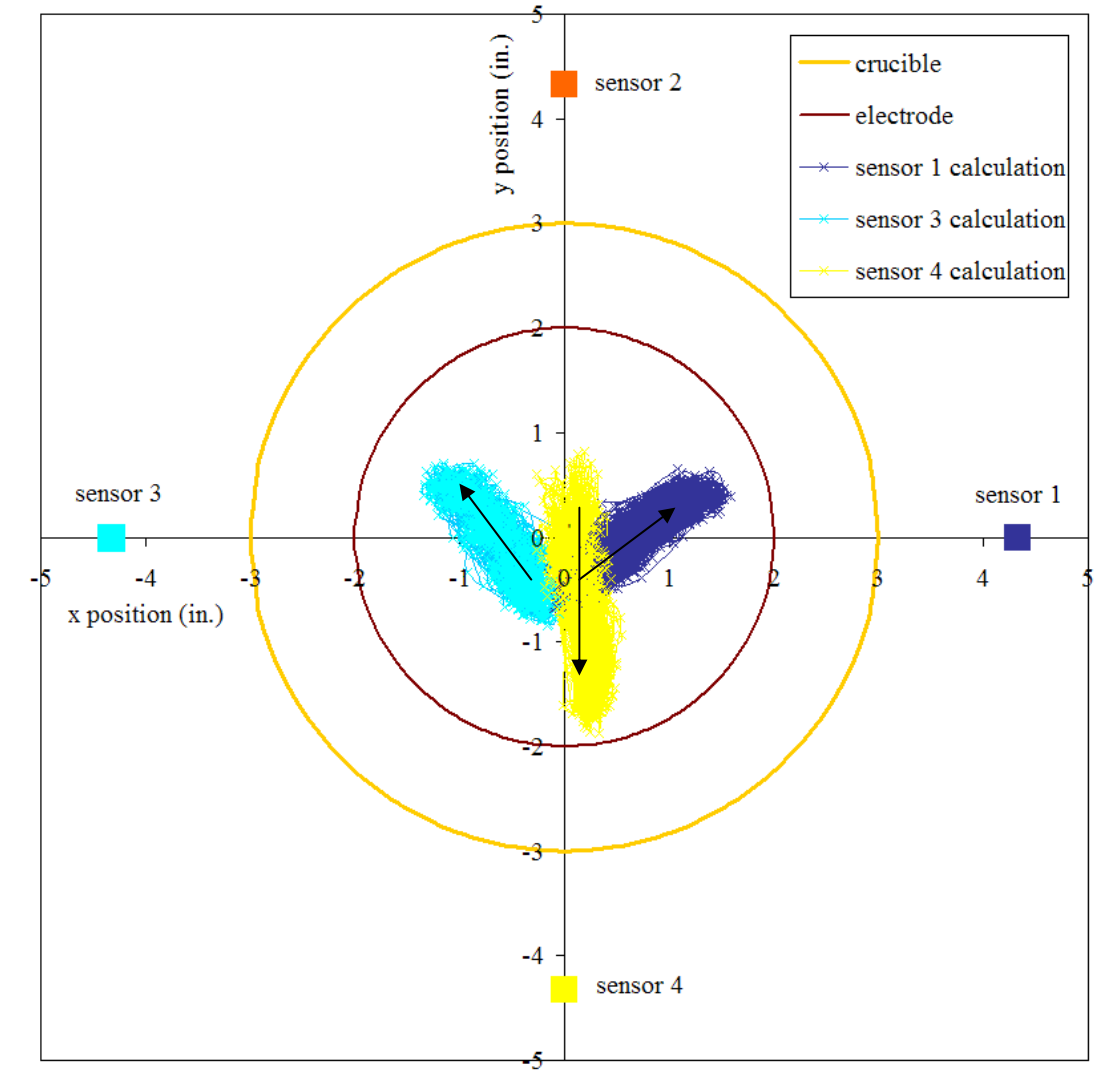

Figure 33 : Instantaneous arc locations for 6-inch In-625 melt sampled at 3000Hz over a 0.5s interval at 1500Amps. Arrows indicate an oscillation direction.

Most of the total distribution area that was previously seen Figure 30 for the 30Hz re-sampled data, actually occurs within a very short time scale. The predicted arc location for each sensor travels from the middle toward the edge in approximately 1ms at a speed of about 50m/s.

Figure 34 shows an FFT of the signals immediately after power is turned on, but before an arc is initiated.

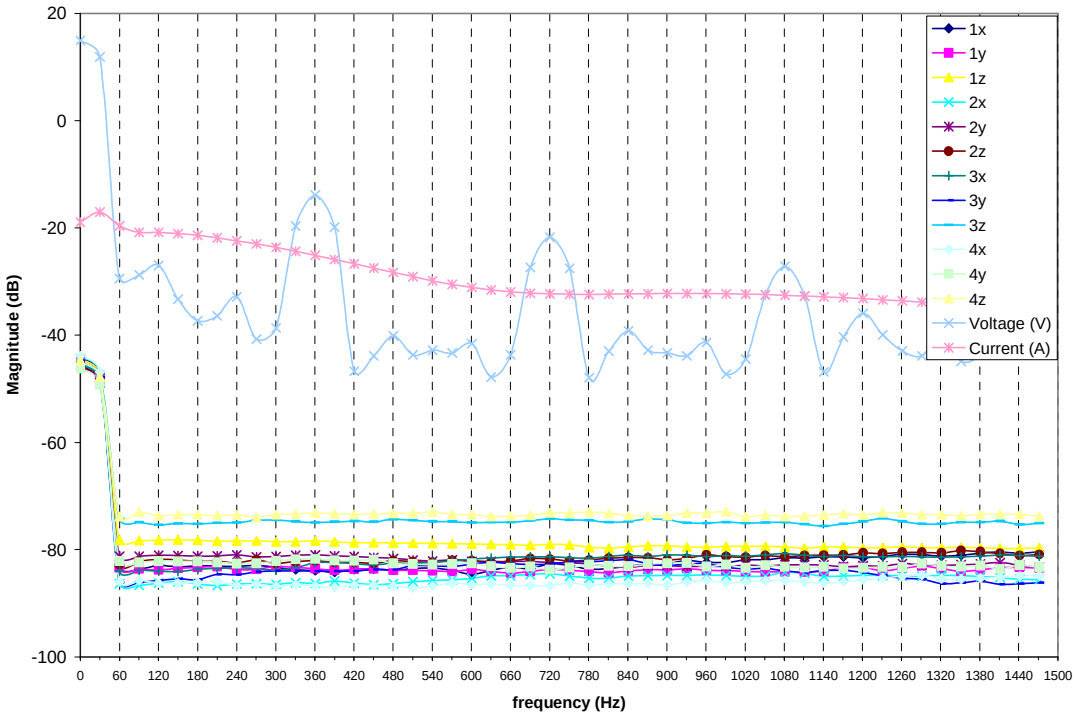

Figure 34 : FFT of 3000Hz data for In-625 melt test #1 over a 1s interval; Power on.

The power supply voltage shows a large signal at 360Hz, and related harmonics. The current jumps up because of the fast transients that randomly occur in the current channel, as discussed in the time domain section. The Hall Effect sensors are unchanged, still showing an even response across the spectrum.

Once current is applied, the same frequency content of the voltage can be seen in the remaining channels. Figure 35 shows the FFT during VAR operation.

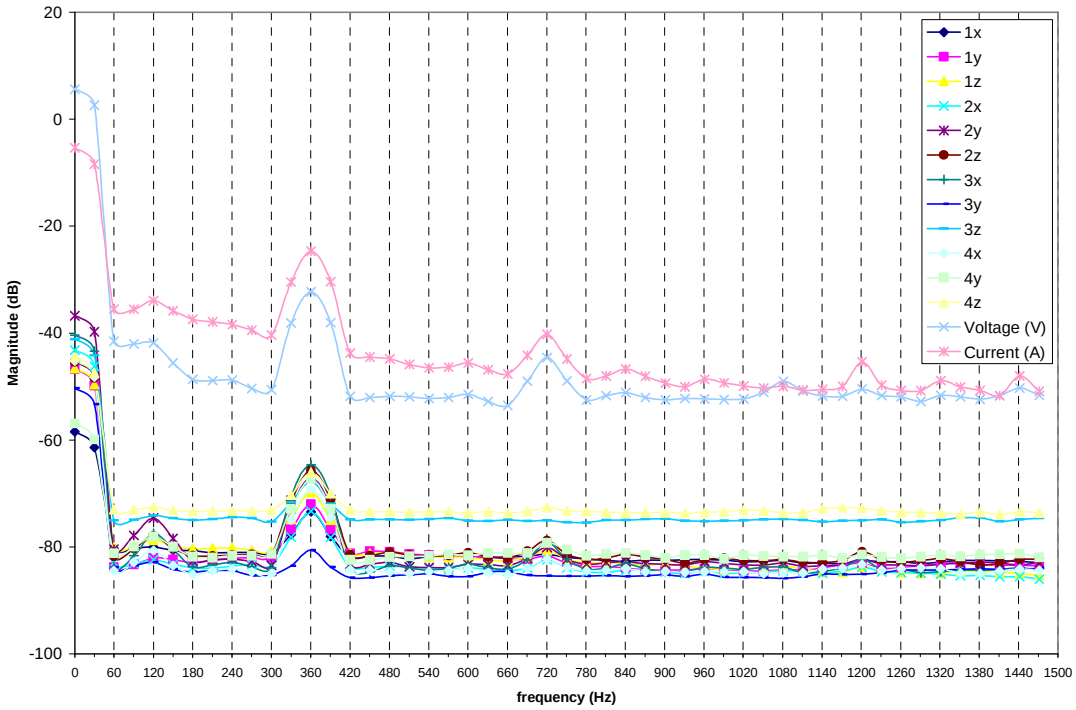

Figure 35 : FFT of 3000Hz data for In-625 melt test #1 over a 1s interval; Melting at 862A.

360 Hz is the main component of oscillation that was seen in Figure 33. Recall that operation of the VAR is supposed to be DC, which is why this result is a bit surprising. Large periodic signals could be a problem for the averaging method used to process the data presented in the time averaged arc location section. So the data was checked by also processing it using a low-pass filter. The resulting distributions were nearly identical to the averaging method, as presented in the time averaged section. Therefore, the periodic signals are oscillating about the mean.

To give an idea of the severity of the AC current, Figure 36 and Figure 37 show 3000Hz data in the time domain. It can be seen that the current oscillates by nearly 1000 Amps about an average of 2500 Amps.

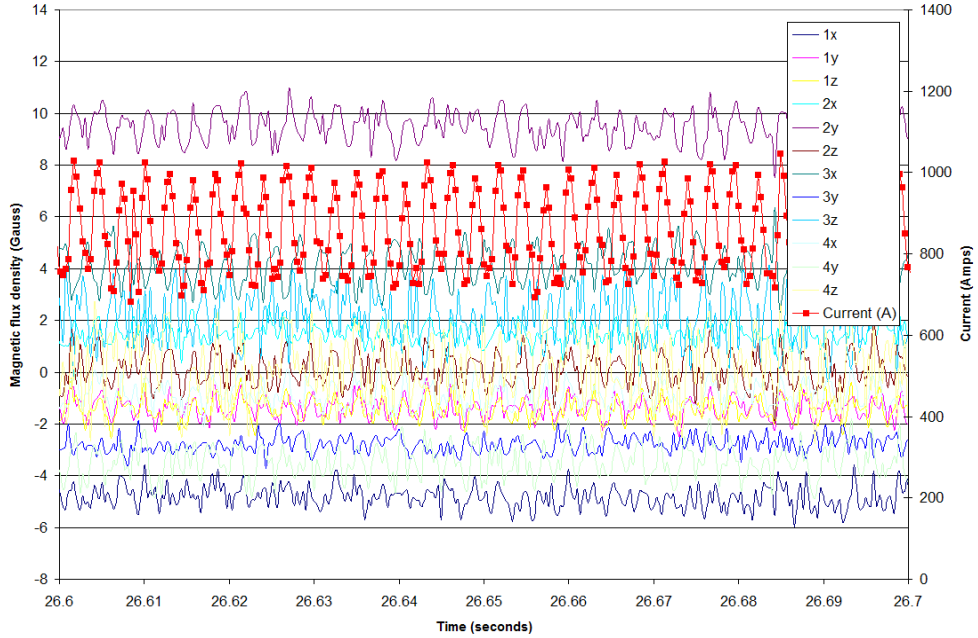

Figure 36 : 3000Hz sampled magnetic flux density and current data versus time for 4-inch In 625 melt #1.

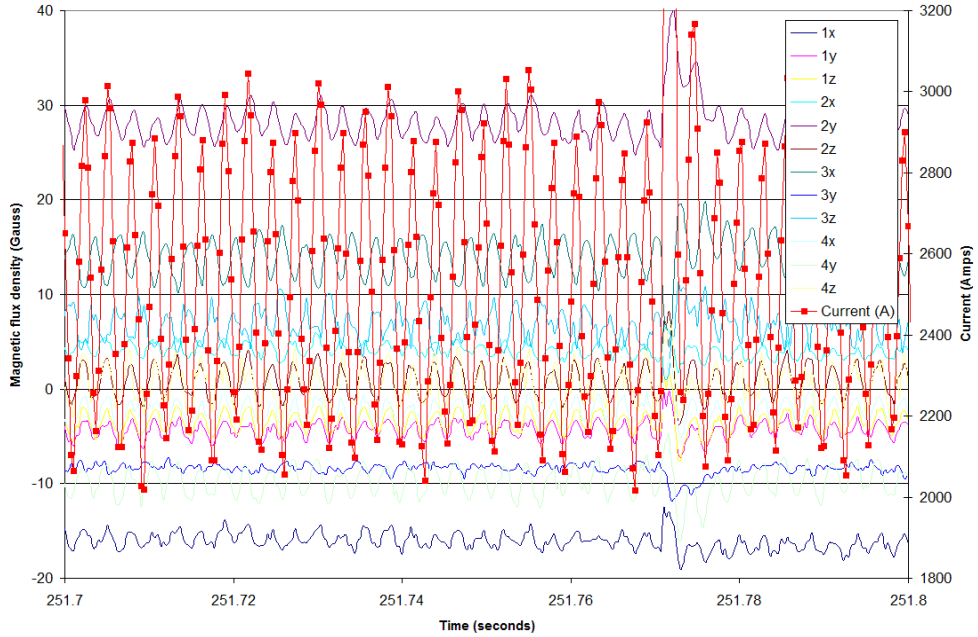

Figure 37 : 3000Hz sampled magnetic flux density and current data versus time for 4-inch In 625 melt #1 with more Amps being applied.

In addition to the current oscillating with a strong 360 Hz component, the magnetic flux density is also oscillating. Further, it appears this data is either in phase or out of phase to the current by approximately 180 degrees. Note that both the DC and AC components of the current increase comparing the data shown in Figure 37 to the data shown in Figure 36.

The FEA simulations showed that the magnetic flux density is linear with the DC current for a given arc position, as would be expected from the equations. The static experiments also verified this. Table 3 shows the parameters for a linear fit to averaged data for the 4-inch In-625 melt test.

Table 3 : *B* vs. *I* linear fit for 4-inch In-625 melt #1 time averaged to 30Hz.

Channel:	1x	1y	1z	2x	2y	2z	3x	3y	3z	4x	4y	4z
slope (Gauss/mA)	-6.24	-1.81	-1.26	1.74	11.02	0.25	5.35	-3.23	2.73	-1.07	-3.80	0.27
y intercept (Gauss)	0.27	0.13	-0.36	0.04	0.20	-0.01	-0.28	0.05	0.19	0.08	-0.31	-0.17
r2 fit	0.97	0.96	0.89	0.94	0.98	0.72	0.97	0.97	0.96	0.91	0.97	0.59

Except for the channels that show very little slope, the r2 fit shows that the data is linear. Table 4 shows what happens when a linear fit is applied to a small window, containing the AC current.

Table 4 : *B* vs. *I* linear fit for 4-inch In 625 melt #1 sampled at 3000Hz over a 1 second interval at 860A.

Channel:	1x	1y	1z	2x	2y	2z	3x	3y	3z	4x	4y	4z
slope (Gauss/mA)	1.78	2.35	2.98	1.93	4.06	5.10	-5.98	-0.70	-3.56	3.54	4.01	4.30
y intercept (Gauss)	-6.44	-3.39	-3.97	-0.11	5.95	-4.21	9.32	-2.17	5.23	-3.89	-6.94	-3.61
r2 fit	0.16	0.34	0.47	0.26	0.45	0.57	0.73	0.06	0.11	0.53	0.38	0.11

The linear fit is not very good, but it is still surprising that the slopes are in most cases the opposite sign of the slope to the averaged data. Table 5 shows the same thing, but for a larger current.

Table 5 : *B* vs. *I* linear fit for 4-inch In 625 melt #1 sampled at 3000Hz over a 1 second interval at 2500A.

Channel:	1x	1y	1z	2x	2y	2z	3x	3y	3z	4x	4y	4z
slope (Gauss/mA)	1.33	1.51	2.01	1.15	2.42	2.72	-3.70	-0.38	-2.17	2.06	2.22	2.80
y intercept (Gauss)	-19.28	-8.20	-8.56	1.47	21.63	-6.22	22.95	-7.18	12.24	-7.79	-15.28	-6.55
r2 fit	0.41	0.48	0.52	0.43	0.37	0.41	0.57	0.10	0.27	0.51	0.37	0.31

Again there is quite a difference in the parameters compared to the DC signals. Also, the y-intercept is different from than the y-intercept for the lower current data but the slopes are only slightly different. This means the AC magnetic flux signal might be following its own independent relationship with current, as might be expected if it were an error due to the magneto static assumption.

By generating sinusoidal signals, similar to the signals seen in Figure 36 and Figure 37, and inputting them into the arc location equations it can be seen that both the magnetic flux density and current oscillations significantly contribute to the predicted retrograde arc motions. In other words, filtering out the AC component in either but not both the current and magnetic flux density data reduces but does not eliminate the predicted motions. Also, the resulting motion is generally in the same direction when considering just the magnetic flux or just the current oscillations.

The NETL “DC” VAR furnaces operate with very significant AC components. These AC components clearly cause the periodic, retrograde motion in the arc location predictions. The directions of the movements are consistent with what would be expected if the analysis was not correctly accounting for changes in current. However, it was also previously shown that multiple, non-axisymmetric arcs could cause retrograde arc motion in the same direction. To further investigate whether the motions are real, the effect of the electric current’s amplitude is examined.

To look at the relationship of the motion to the amplitude of the current over the duration of a melt, the sensor 4 y-axis data from Figure 30 is presented in the time domain with the current data. Sensor 4 was chosen for convenience because the oscillation is almost exclusively in the y-direction. This data can be seen in Figure 38.

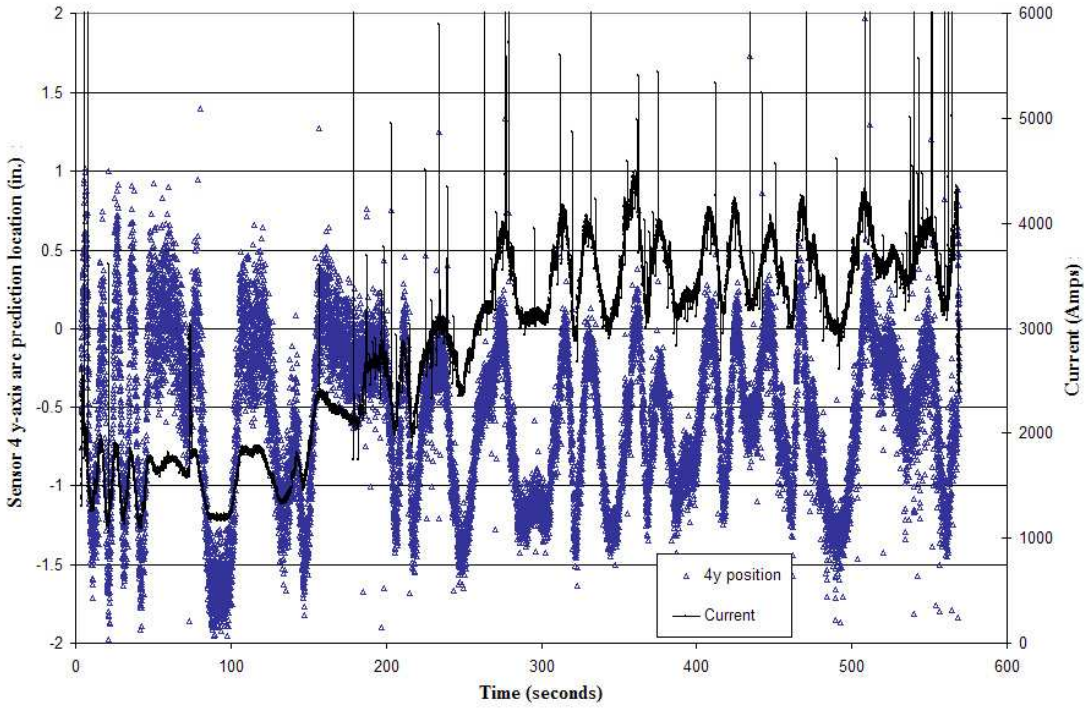

Figure 38 : Sensor 4 y-axis arc location predictions and current data for 6-inch In 625 melt. The data was re-sampled to 30Hz, causing higher frequencies to alias.

By re-sampling the data to 30Hz, the 360 Hz and related harmonics of the current and arc motion alias to much lower frequencies. Aliasing is an artifact caused by discrete sampling of a signal whereby any frequencies above the Nyquist frequency of twice the sampling rate will appear as a signal component having much lower and false frequency content. The amplitude of the signal at any given data point will not be affected by this aliasing, so it is still useful to look at this data.

It can be seen that the predicted y-axis location does not appear to significantly respond to either the increase in DC current, or the increase in AC current. Analyzing the oscillations from the other sensors and for the other experiments yields the same result. This is significant because not only does the amplitude of current increase, but so does the rate of change of the current (the frequency is still primarily 360 Hz). Both of which are important in electromagnetic equations. If the oscillation were actual motion of arcs, then there is a limited distance of travel dictated by the diameter of the

electrode. This would cause the oscillation amplitude to remain constant versus current. Considering this, the retrograde oscillation could be a genuine mode of arc motion in the furnace.

Still, dynamic electromagnetic analysis would be needed to definitively conclude whether this motion is real. It is likely that neglecting the displacement current and other dynamic effects contributes to the observed retrograde arc motions to some degree. However, it seems unlikely that these effects would cause an error in the quasi static approach in which the oscillations remained constant versus current.

Also of interest, is that the frequency of the aliased signal does not appear to be entirely consistent. Aliasing will occur at a consistent and predicable frequency. The changing frequency seen in the aliased data therefore suggests that the relationships between the amplitudes of AC harmonics are not entirely consistent throughout the melt.

Periodic behavior of the VAR and power supply was not expected, and there remains more to be investigated. Ultimately, dynamic electromagnetic analysis will be needed to fully investigate instantaneous and periodic arc behavior, which is outside the scope of the present work.

Random Sympathetic Arc Motions

After removal of the high frequency retrograde motion content via averaging, it was observed that there was a different kind of motion present. This low frequency motion is sympathetic in that the separate sensors agree on the direction and magnitude of the movements. The movements are relatively small, occurring over amplitudes of about 0.1 inches. The direction of travel also does not appear to be static, but rather it changes over the course of the melt. Also, the motions appear to be largely random, as opposed to periodic like the retrograde motions. Larger sympathetic arc motions were also observed, but these seem to correspond to events such as drip shorts, and will be looked at in the next section.

The easiest way to demonstrate sympathetic movement is to look at the prediction map versus time, which is done in the LabVIEW VI. This shows that the sensor's predictions tend to move together.

The sympathetic movements are small so they need to be differentiated from what might be expected from random noise. To get an idea on what the sensor's noise looks like, a histogram of the data for one of the sensors is shown in figure 41. This is with the VAR's power off.

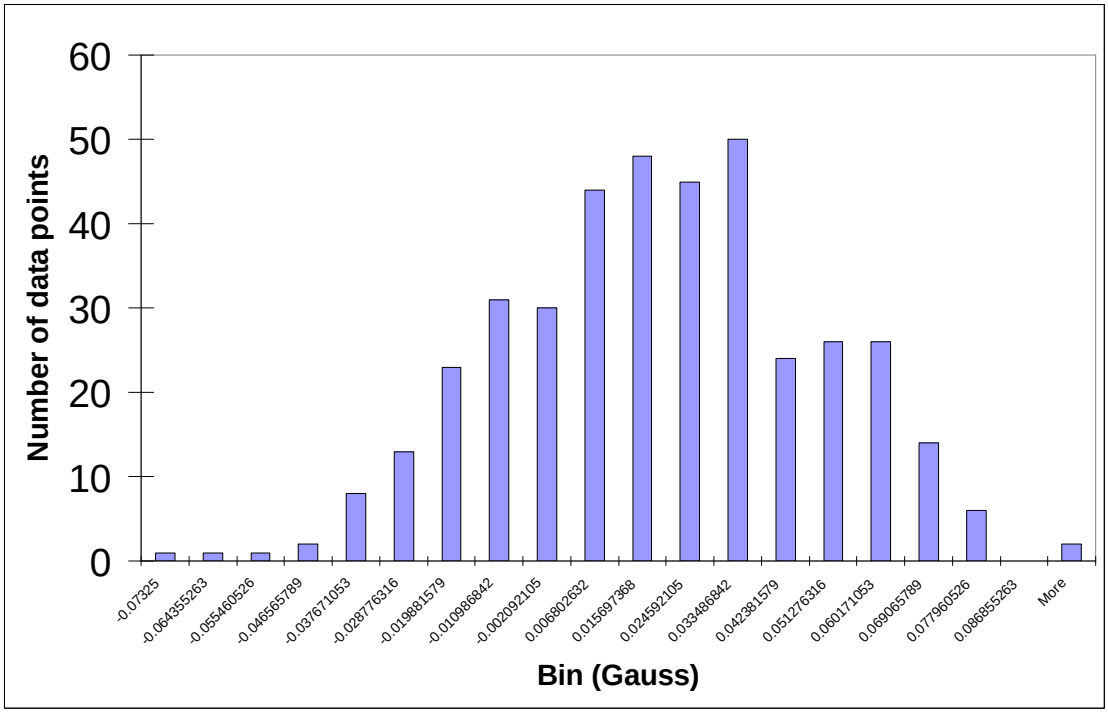

Figure 39 : Noise of channel 4y at 0V, 0A

The noise has a Gaussian shape to it, which is expected from electronics showing Johnson, or thermal noise. To quantify a parameter to describe this noise, a standard deviation is used. Table 6 shows the standard deviations of the acquired signals at 4 separate 1 second intervals during one of the experiments.

Table 6: Standard deviations of the measurements. Data shown is for the 4-inch In-625 melt #1 using 30 Hz averaged data over a 1 second interval

std.dev. (Gauss):	1x	1y	1z	2x	2y	2z	3x	3y	3z	4x	4y	4z	Volts	Amps
off: 0V, 0A	0.05	0.03	0.03	0.02	0.02	0.02	0.03	0.02	0.12	0.03	0.05	0.14	0.00	0.13
on: 60 V, 0A	0.04	0.03	0.02	0.03	0.03	0.03	0.03	0.03	0.12	0.02	0.05	0.14	0.55	0.23
on: 860 A	0.09	0.04	0.04	0.08	0.07	0.04	0.09	0.05	0.12	0.05	0.06	0.13	0.05	4.04
on: 2500 A	0.30	0.11	0.05	0.28	0.28	0.09	0.29	0.12	0.12	0.23	0.15	0.15	0.11	14.88

The noise is very miniscule with the VAR off, at around 0.03 Gauss. It was ensured that none of the standard deviation calculations were skewed by an event such as a drip short. The standard deviation for each channel increases with increasing current. This could be due to inadequate averaging of the periodic AC components, an unknown convolved noise source, or it could be actual movement of the arc and changes in the electrode gap resistance.

To differentiate sympathetic motion from random noise, a simulation was employed. This involved simulating both the magnetic flux density and current with a Gaussian type random generator with a standard deviation identical to the values shown in Table 6. Figure 40 shows the resulting arc locations for the simulation. Also, shown is actual data from the average data set that has the same standard deviation.

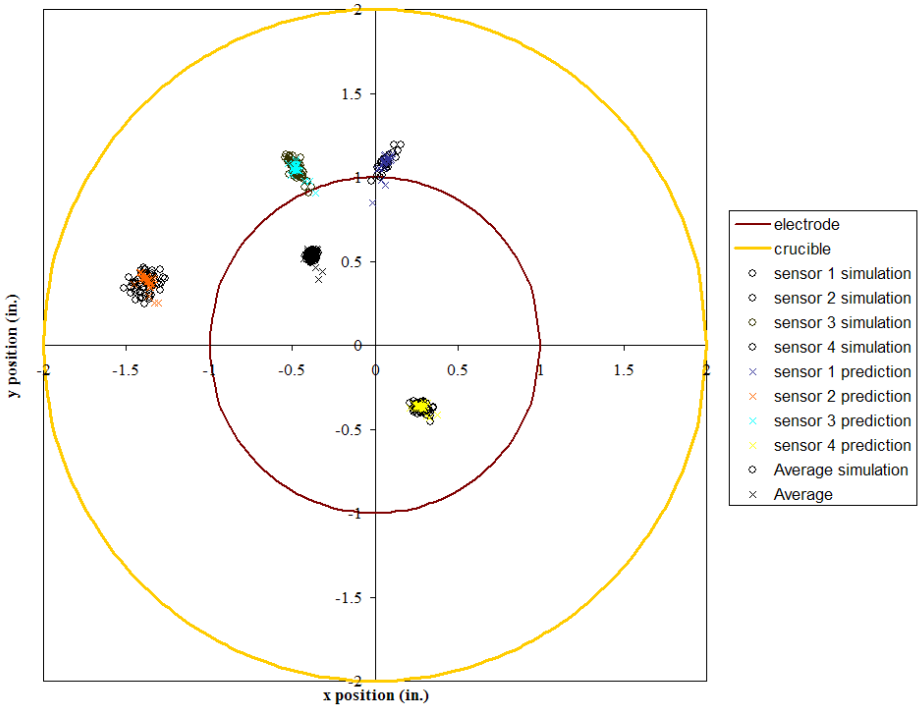

Figure 40 : Simulation of Gaussian *B* and *I* noise and comparison to calculations over 1 second interval.

The data shown in Figure 40 was from an analytically based solution, as this analysis was performed prior to the fully developed FEA assisted solution presented in this study. Results for this analysis are not mentioned because they are similar to the final solution used in terms of motion, with some differences in the absolute locations of the predictions.

It can be seen that simulating random Gaussian type noise can yield a distribution that is nearly identical to the actual data. However, the difference between the random simulated data and the measured data can be seen when comparing sensors in the time domain. To demonstrate this, the derivatives of each sensor's predictions from the actual data and from the random noise simulation were taken for both the x and y directions. Then, the standard deviations of the four sensors were taken for the prediction and for the simulation. Thereby sympathetic movements will have a low

standard deviation, meaning the sensors agree on the movement amount and direction. Figures 43 and 44 show this parameter for the x and y direction, respectively.

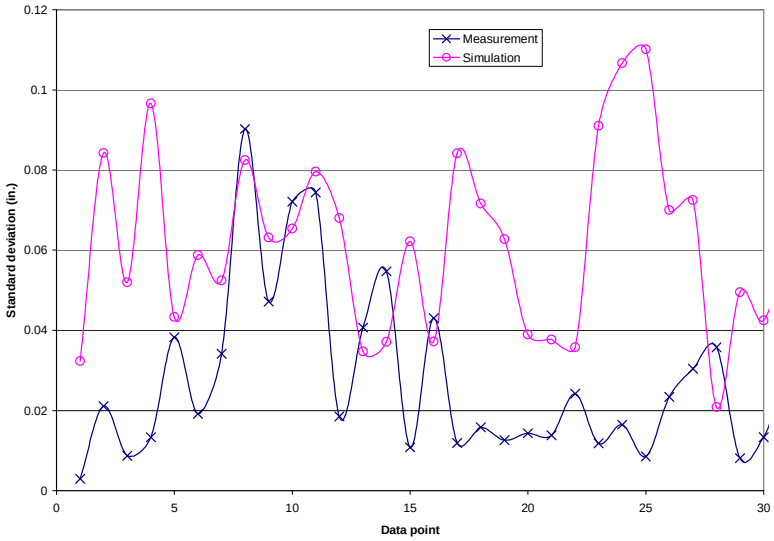

Figure 41 : Plotting the four sensor standard deviation of the derivative of the predicted motion and the simulated noise motion for the x-direction. A low value indicates sympathetic motion.

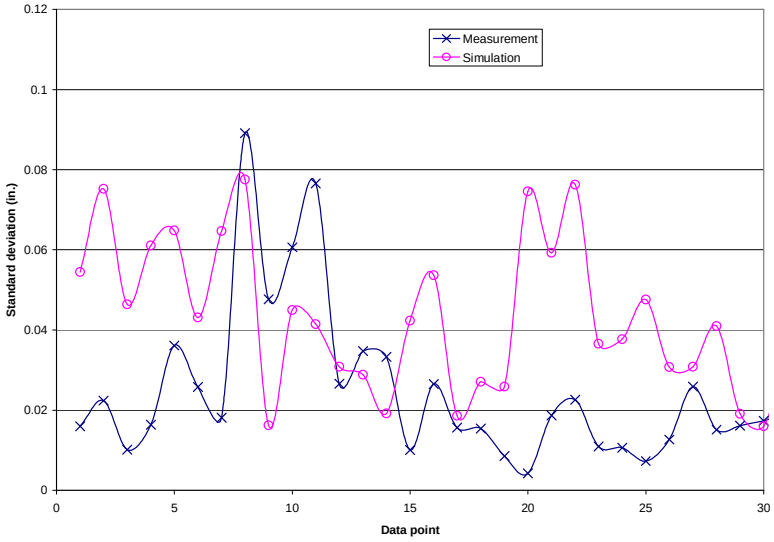

Figure 42 : Plotting the four sensor standard deviation of the derivative of the predicted motion and the simulated noise motion for the y-direction. A low value indicates sympathetic motion.

The standard deviations of the derivatives very clearly show that the actual data shows sympathetic movement between sensors compared to a simulated random noise data set. This is good evidence that the measurement system is measuring small scale vibrations in arc location, and not just registering noise. Of course, motion is relative, so a crucible vibrating in relation to the outside of the chamber could yield a similar result.

Event Sympathetic Arc Motions

In addition to the low amplitude vibration type sympathetic motion observed, the sensors also agreed on the direction of motion corresponding to events. These events occurred every second or so, at a time interval that seems consistent with what might be expected with drip shorts. Also, they largely corresponded to a current surge event.

Correlation of the video to the sensor data was unfortunately not feasible for an entire melt. This was because of time alignment issues between the images and the sensor data. The timing between the video and the data was done via software, and the total number of data points taken did not exactly correspond to the expected number of video frames.

However, the data could be synchronized with confidence near the ends of the experiments. This was because the event of shutting off the current corresponded to a sharp reduction of light from the furnace. The 6-inch In 625 had an eventful ending that involved unstable arc conditions and ultimately the electrode fell off the stinger attachment and into the melt pool. This series of events clearly show activity at the edge of the electrode to correlate to, and also allowed for capture of images of an arc.

Plotting the 4 sensor independent arc location prediction dots on top of the video frames allows a clear picture of the movement of the dots toward the area of the event. Figure 43 shows an event on the north side of the furnace.

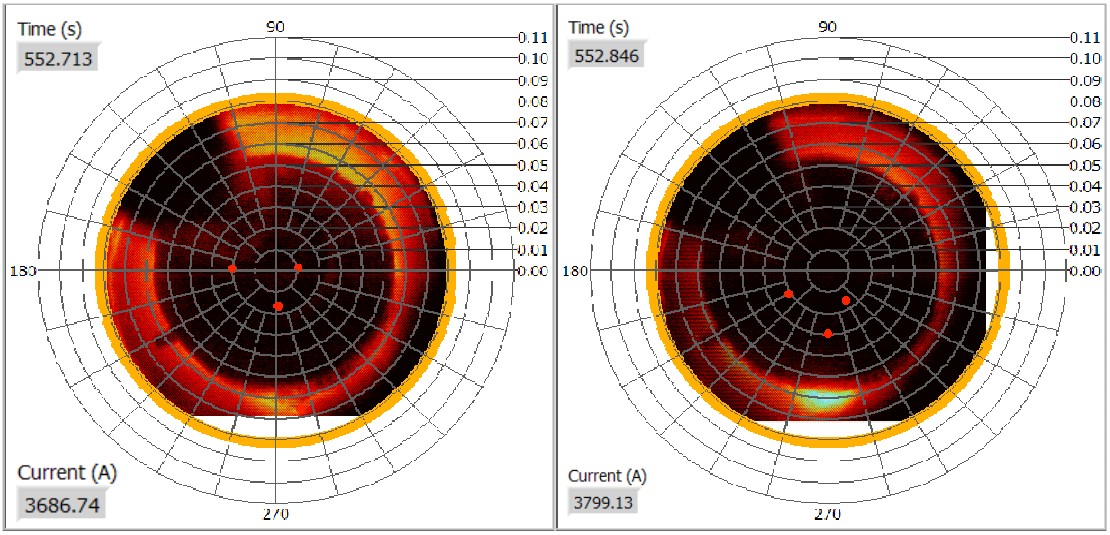

Figure 43 : Arc location predictions superimposed on video for event 1. The two frames taken are from the end of 6-inch In-635 melt.

Figure 44 shows an event in the same direction, but more towards the east. The event appears as a bright spot on the edge of the electrode.

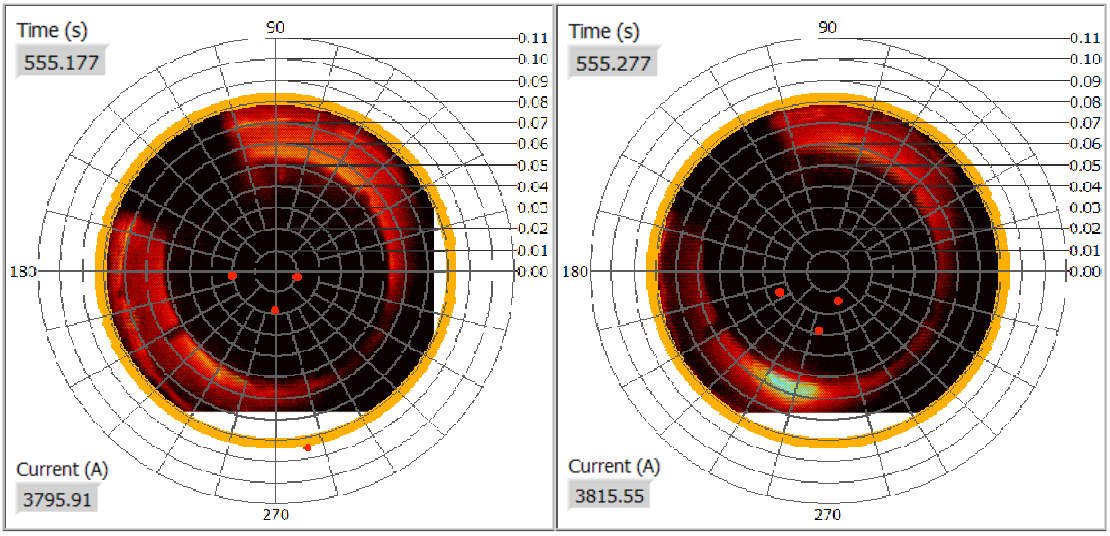

Figure 44 : Arc location predictions superimposed on video for event 2. The two frames taken are from the end of 6-inch In-635 melt.

Figure 45 shows an event where it appears the arc is actually coming out at an angle from the electrode to the melt pool on the east side.

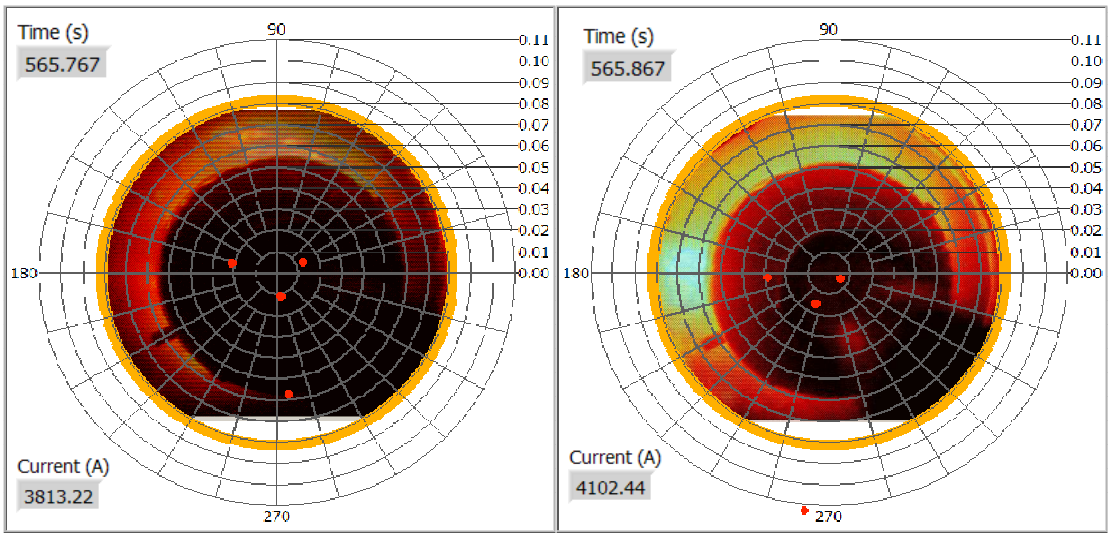

Figure 45 : Arc location predictions superimposed on video for event 3. The two frames taken are from the end of 6-inch In-635 melt.

Figure 46 shows the electrode before and after it falls into the melt pool. An arc can actually be seen as it follows the electrode into the south side of the melt pool. Again, the predicted arc locations move in the expected direction.

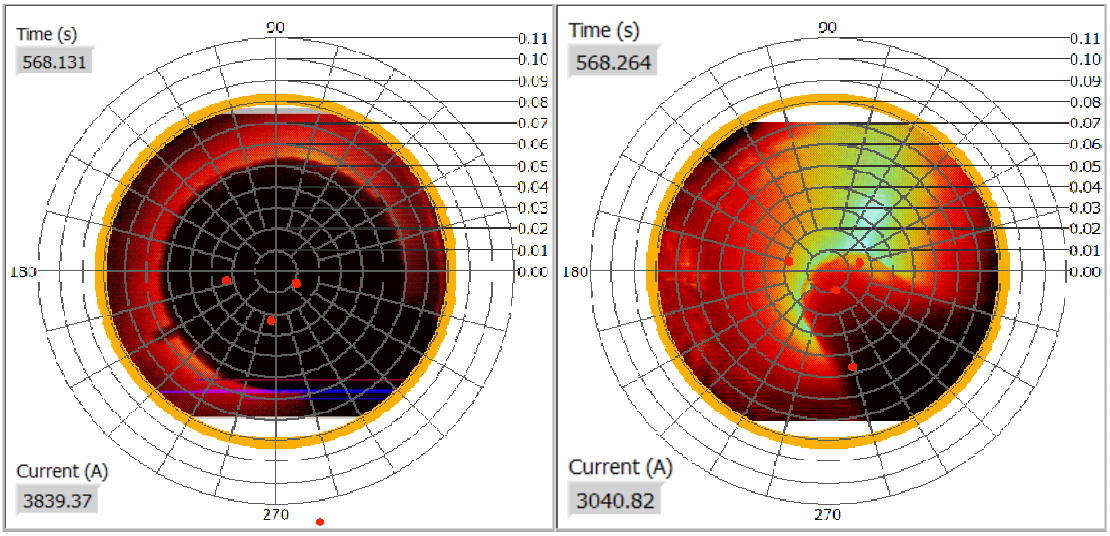

Figure 46 : Arc location predictions superimposed on video for event 4. The two frames taken are from the end of 6-inch In-635 melt.

The video clearly shows events that draw the arc to one side or another. The predictions for each sensor follow in the right direction, showing the analysis technique is working. However, the movement does appear to be attenuated.

The predictions plotted used the time averaged 30Hz data set. Previous analysis has shown that there is not a great deal of attenuation due to this averaging, and also events were chosen that appeared to last more than one video frame. The video was taken at 30 frames per second. The attenuation could be a result of not accounting for the movement of current through the plasma. There may be a significant amount of current moving through the diffuse plasma cloud, which would cause an overall non-directional attenuation of predicted arc event movements, as is observed. Further study could model the electrical conductivity of the plasma using the FEA, to see if this can resolve this attenuation error.

Conclusions

This thesis describes the instrumentation and analysis techniques for characterizing arc behavior using externally mounted magnetic flux density sensors. One of the primary purposes of the study was to investigate whether this could provide useful information to VAR operation. To this end, the technique is worth pursuing.

Energy input into the ingot pool is of interest to operation because it is information that directly impacts the formation of defects. This information cannot be obtained with currently used VAR instrumentation techniques. The use of external magnetic field sensors can potentially map this energy input during operation. Although instantaneous arc location predictions are still not possible, the time averaged results are promising indicators. This allows for near real time identification of non-axisymmetric behavior, and can identify whether there are spatial variations over time. Further, the use of four individually analyzed 2-axis Hall Effect sensors mounted on opposite sides of the furnace has a desirable effect in reducing a variety of errors that might be encountered by the measurement system. For example, errors in current variation cancel out.

By comparing predictions from multiple sensors, the observed motions of the arc are categorized as either being retrograde or sympathetic. Retrograde, or opposing, motion is characterized by the motion being canceled out when the arc location predictions from separate sensors are averaged. Sympathetic motion, on the other hand, is characterized by the separate sensors generally agreeing on the direction and magnitude of motion. Further experimentation and analysis is needed to explain the mechanisms behind the observed motions.

The following general conclusions can be made as a result of this work. Observations regarding VAR arc behavior may be specific to the one studied at NETL.

1. Data from a single 2-axis Hall Effect sensor can be used to exactly determine the location of a current source in a cross section of a VAR with known geometry if the magnitude of that current is known.
2. The time averaged arc location plot is effective at identifying non-axisymmetric constricted arcs. The NETL VAR routinely operates with constricted arc conditions, likely due to the bus bar being parallel and in close proximity to one side of the furnace.
3. No ensemble arc motion was observed. The time averaged distributions remained constant over the duration of the experiments, although the melts were only approximately 10 minutes in duration. No time varying behavior was seen as might occur in the presence of periodic boundary condition changes between the ingot and the crucible.
4. The single arc assumption, the magneto static equations, or both are not valid to describe arc conditions at an instant. Dynamic electromagnetic analysis could provide further insight.
5. Using multi axis Hall Effect sensors to characterize the arc as described cannot practically measure the difference between multiple arcs that are axisymmetric and a single arc that is constricted to the exact middle.
6. Frequency content of the power supply plays a significant role in driving the observed periodic and retrograde VAR arc motions.
7. Motions of the arc exist that are low in amplitude of around 0.1 inches, and at frequencies below 15 Hz. The cause is not clear, though mechanical vibrations could be implicated.
8. Multi axis Hall Effect sensors can be used to locate the position of an event such as metal transfer drip shorts. The observed attenuation of motion associated with these events could be reduced if the current that diffusely moves through the plasma is taken into account.

The developed mathematics for remote detection of arc location was verified using controlled static experiments using an electrode placed at known locations in the

VAR furnace. The static tests also showed the robustness of the technique to changes in current, as no significant changes in the location of the predictions were seen due to increasing current.

The measurement technique using magnetic flux density sensors has advantages in that it is non-destructive and can be adapted to fit on existing furnaces for low cost. Additionally, analysis is performed in LabVIEW in a way that allows for real time tracking of the arc. Identical melting geometries show similar responses, showing that a single FEA model is needed for each crucible and electrode geometry configuration.

Ultimately, it will be necessary to test the measurement system on a large scale VAR because operation of these VAR furnaces provides the motivation behind the research. The time averaged method may be a useful tool as it is described in this thesis. Full understanding of process and realization of an instantaneous arc location prediction will likely require moving away from the fully deterministic method to principles used in magnetic tomography. Full transient electromagnetic equations may also be needed. Combining principles of tomography with selective and directional magnetic shielding of sensor elements should allow for a detailed map of the current flow through a cross section at an instant to be measured. It has been mathematically shown that the current densities can be reconstructed inside a volume if the magnetic flux density on the surrounding surface of the volume is known.[25]

Bibliography

1. Zanner, F., Williamson, R., and Erdmann, R. *On the Origin of Defects in VAR ingots*, Liquid Metals Processing and Casting, (2005).

2 *United Airlines Flight 232*, Wikipedia, The Free Encyclopedia, December 25, 2007. <http://en.wikipedia.org/wiki/United_Airlines_Flight_232>

3. Schafrik, Robert, and Sprague, Robert. *Saga of Gas Turbine Materials Part 4* Advanced Materials & Processes, (2004): 41-46.

4. King, Paul E., *Magnetohydrodynamics in Electric Arc Furnace Steel Making*, Report of Investigations 9320, US Bureau of Mines, (1990).

5. Van Den Avyle, Brooks, John A., and Powell, Adam. "*Reducing Defects in Remelting Processes for High-Performance Alloys*," JOM (1998): 22-26.

6. Chen, W., Yang W.H., Chang, K., Mannan, S.K., and deBarbadillo, J.J. *Examination of Freckles in a Remelted Niobium Containing Nickel Base Superalloy*, Liquid Metals Processing and Casting, (1999).

7. Jackman, L.A., Maurer, G.E., and Widge, S. *White Spots in Superalloys, superalloys 718,625,706 and various derivatives*, E.A. Loria ed. TMS (1994):153-166.

8. Xu, X., Ward R.M., Jacobs, M.H., Lee, P.D., and McLean, *Tree Ring Formation during VAR of Inconnel 718: Part 1. Experimental Investigations*, Metallurgy transactions A. Volume 33A, (2002):1795-1803.

9. Xu, X., Ward R.M., Jacobs, M.H., Lee, P.D., and McLean, *Tree Ring Formation during VAR of Inconnel 718: Part 2. Experimental Investigations* Metallurgy transactions A, Volume 33A, (2002):1795-1803.

10. Zanner, F.J. *Observation of the Vacuum Arc and Metal Transfer during Vacuum Consumable Arc Remelting*. Proceedings of the International Conference on Special Melting (1979):417-427.

11. Zanner, F.J. *Vacuum Consumable Arc Remelting Electrode Gap Control Strategies Based on Drop Short Properties*, Metallurgical Transactions B, 12B (1981):721-728.

12. Zanner, F.J., Adasczik, C., O'brien, T., and Bertam, L.A. *Observations of melt rate as a function of arc power, CO pressure, and electrode gap during vacuum consumable arc remelting of Inconnel 718*, Metallurgical Transactions B, 15B (1984): 117-125.

13. Bellan, Paul M., U.S. Patent 4,815,097.

14. Heberlein V, Joachim R. and Fey, Maurice G., U.S. Patent 4,495625.

15. Melgaard, D.K., Willimason, R.L., and Beaman, J.J. *Controlling remelting processes for superalloys and aerospace Ti alloys*, JOM (1998):13-17.

16. Reece, M.P., *The Vacuum Switch—Part 1. Properties of the Vacuum Arc*, Proc. Inst. Elec. Eng. Volume 110, (April 1963):793-802.

17. King, Paul E., *ELECTRO-MAGNETO-HYDRODYNAMICS: The process of Electric Arc Steelmaking*, Oregon State University Masters Thesis, OR, (1988).

18. Bertram, L.A., Zanner, F.J. and Marder, B.M. *Current Paths and MHD in Vacuum Arc Remelting*, Single-and Multi-Phase Flows in an Electromagnetic Field Energy, Metallurgical, and Solar applications (1985): 617-633.

19. Zanner, F.J. *Metal Transfer During Vacuum Consumable Arc Remelting.* Metallurgical Transactions B 10B (1979):133-142.

20. Griffiths, David J., *Introduction to Electrodynamics*, Prentice-Hall, Inc. Englewood Cliffs, NJ, (1981).

21. Ward, R.M., Daniel, B., and Siddall, R. J. *Ensemble Arc Motion and Solidification During the Vacuum Arc Remelting of a Nickel-based Superalloy,* Liquid metals processing and Casting, (2005).

22. Bertam, L.A., and Zanner, F.J. *Electrode Tip melting Simulation during vacuum arc remelting of inconel 718,* unpublished, Sandia National Laboratories.

23. Williamson, R.L., Shelmidine G.J., and Maroone, J.P. *Current Profiles During VAR of Ti-5Al-4V,* Liquid Metals Processing and Casting, (2005).

24. *Comsol Multiphysiscs 3.2 users guide*, (2005).

25. Kress, Rainer, Kuhn,Lars, and Potthast, Roland. *Reconstruction of a current distribution from its magnetic field,* Inverse Problems 18 (2002):1127-1146.